


Istaroxime Metabolite PST3093 Selectively Stimulates SERCA2a and Reverses Disease-Induced Changes in Cardiac Function[§]

Martina Arici,¹ Mara Ferrandi,¹ Paolo Barassi, Shih-Che Hsu, Eleonora Torre, Andrea Luraghi, Carlotta Ronchi, Gwo-Jyh Chang, Francesco Peri, Patrizia Ferrari, Giuseppe Bianchi,  Marcella Rocchetti,² and Antonio Zaza²

Department of Biotechnology and Biosciences, Università degli Studi di Milano-Bicocca, Milan, Italy (M.A., E.T., A.L., C.R., F.P., M.R., A.Z.); Windtree Therapeutics Inc., Warrington, Pennsylvania (M.F., P.B., P.F., G.B.); CVie Therapeutics Limited, Taipei, Taiwan (S.-C.H.); Graduate Institute of Clinical Medicinal Sciences, College of Medicine, Chang Gung University, Tao-Yuan, Taiwan (G.-J.C.); and Università Vita-Salute San Raffaele, Milan, Italy (G.B.)

Received May 30, 2022; accepted August 1, 2022

ABSTRACT

Heart failure (HF) therapeutic toolkit would strongly benefit from the availability of ino-lusitropic agents with a favorable pharmacodynamics and safety profile. Istaroxime is a promising agent, which combines Na⁺/K⁺ pump inhibition with sarcoplasmic reticulum Ca²⁺ ATPase (SERCA2a) stimulation; however, it has a very short half-life and extensive metabolism to a molecule named PST3093. The present work aims to investigate whether PST3093 still retains the pharmacodynamic and pharmacokinetic properties of its parent compound. We studied PST3093 for its effects on SERCA2a and Na⁺/K⁺ ATPase activities, Ca²⁺ dynamics in isolated myocytes, and hemodynamic effects in an in vivo rat model of diabetic [streptozotocin (STZ)-induced] cardiomyopathy. Istaroxime infusion in HF patients led to accumulation of PST3093 in the plasma; clearance was substantially slower for PST3093 than for istaroxime. In cardiac rat preparations, PST3093 did not inhibit the Na⁺/K⁺ ATPase activity but retained SERCA2a stimulatory activity. In in vivo echocardiographic assessment, PST3093 improved overall cardiac performance and reversed most STZ-induced abnormalities. PST3093 intravenous toxicity was considerably lower than that of istaroxime, and it failed to significantly

interact with 50 off-targets. Overall, PST3093 is a “selective” SERCA2a activator, the prototype of a novel pharmacodynamic category with a potential in the ino-lusitropic approach to HF with prevailing diastolic dysfunction. Its pharmacodynamics are peculiar, and its pharmacokinetics are suitable to prolong the cardiac beneficial effect of istaroxime infusion.

SIGNIFICANCE STATEMENT

Heart failure (HF) treatment would benefit from the availability of ino-lusitropic agents with favourable profiles. PST3093 is the main metabolite of istaroxime, a promising agent combining Na⁺/K⁺ pump inhibition and sarcoplasmic reticulum Ca²⁺ ATPase2a (SERCA2a) stimulation. PST3093 shows a longer half-life in human circulation compared to istaroxime, selectively activates SERCA2a, and improves cardiac performance in a model of diabetic cardiomyopathy. Overall, PST3093 as a selective SERCA2a activator can be considered the prototype of a novel pharmacodynamic category for HF treatment.

This research was supported by CVie Therapeutics Limited (Taipei, Taiwan), WindTree Therapeutics (Warrington, PA), and University of Milano Bicocca. This work received no external funding.

M.F. and P.B. are Windtree employees, P.F. and G.B. are Windtree consultants, and S.-C.H. is an employee of CVie Therapeutics Limited. All the other authors declare no conflicts of interest.

¹M.A. and M.F. contributed equally to this work as first authors.

²M.R. and A.Z. contributed equally to this work as senior authors.

dx.doi.org/10.1124/jpet.122.001335.

[§] This article has supplemental material available at jpet.aspetjournals.org.

Introduction

Heart failure (HF) is characterized by abnormal Ca²⁺ distribution among subcellular compartments, which contributes to impaired contractility and relaxation (Bers and Despa, 2006), facilitates arrhythmias (Zaza and Rocchetti, 2015), and, in the long run, contributes to myocardial remodeling (Nakayama et al., 2007). Evidence of a deficient sarcoplasmic reticulum Ca²⁺

ABBREVIATIONS: a', peak late diastolic tissue velocity; A, late diastolic transmitral flow velocity; AP, action potential; APD, action potential duration; APD₅₀, AP duration at 50% repolarization; APD₉₀, AP duration at 90% repolarization; AUC_{last}, the area under the curve from the start of drug administration to the time of final sampling; Ca_{rest}, resting Ca²⁺ at 20-second pause end; Ca_{SR}, SR Ca²⁺ content; CaT, Ca²⁺ transient; CO, cardiac output; DT, deceleration time; e', peak early diastolic tissue velocity; E, early diastolic transmitral flow velocity; E_{diast}, diastolic potential; EDV, end-diastolic volume; EF, ejection fraction; ER, excitation-release; ESV, end-systolic volume; FS, fractional shortening; HF, heart failure; HR, heart rate; I_{CaL}, L-type Ca²⁺ current; I_{NaK}, Na⁺/K⁺ ATPase current; IVSTd, interventricular septal thickness in diastole; IVSTs, interventricular septal thickness in systole; K_{dCa}, Ca²⁺ dissociation constant; LV, left ventricle; LVEDD, LV end-diastolic diameter; LVESD, LV end-systolic diameter; N, number of animals; n, number of cells; NCX, Na⁺/Ca²⁺ exchanger; PK, pharmacokinetic; PLN, phospholamban; PWTd, posterior wall thickness in diastole; PWTs, posterior wall thickness in systole; RM, repeated measurement; SERCA, sarcoplasmic reticulum Ca²⁺ ATPase; SR, sarcoplasmic reticulum; STV, short-term variability; STZ, streptozotocin; SV, stroke volume; s', peak systolic tissue velocity; t_{0.5}, time for 50% Ca²⁺ transient decay; T_{0.5}, drug elimination half-life time; T_{max}, the time of maximum observed concentration; τ, time constant.

ATPase2a (SERCA2a) activity in HF dates to the 1970s (Suko et al., 1970; Sulakhe and Dhalia, 1971). Since then, many studies confirmed this finding (Gwathmey et al., 1987; Arai et al., 1993; Kranias and Hajjar, 2012) showing that the impaired SERCA2a activity can often result from an over-inhibition by phospholamban (PLN) (Haghighi et al., 2001; Del Monte et al., 2002). Loss of SERCA2a function accounts for abnormal distribution of intracellular Ca^{2+} , with numerous detrimental consequences. Interventions currently available to modulate myocyte Ca^{2+} handling (e.g., amines, PDE inhibitors, etc.) stimulate SERCA2a, but they do so in the context of a multi-target action, thus resulting in untoward effects. Selective SERCA2a enhancement would afford inotropic and lusitropic effects without the drawbacks of the multitarget action (Zaza and Rocchetti, 2015). Accordingly, the use of SERCA2a stimulation in HF therapy is receiving considerable attention, and many attempts to selectively stimulate SERCA2a activity with gene therapy or “small molecule” agents have been reported (Kho et al., 2011; Kaneko et al., 2017; Schaaf et al., 2020). Nonetheless, for reasons other than refutation of the principle, none of these attempts has been successfully translated into the clinic. The only exception is istaroxime, a small-molecule drug, identified as a SERCA2a enhancer by our group (Rocchetti et al., 2005) and currently under clinical development for the treatment of acute HF (Shah et al., 2009; Carubelli et al., 2020). Istaroxime has a double mechanism of action: it inhibits the Na^+/K^+ pump (Micheletti et al., 2002) and activates SERCA2a (Rocchetti et al., 2005). Thus, istaroxime increases overall cell Ca^{2+} content while promoting rapid Ca^{2+} sequestration into the sarcoplasmic reticulum (SR). Notably, at variance with Na^+/K^+ pump blockade alone, this neither facilitates spontaneous Ca^{2+} release from the SR (Alemanni et al., 2011) nor increases myocardial oxygen demand (Sabbah et al., 2007). Thus, istaroxime may improve systolic and diastolic performance (Shah et al., 2009) without promoting arrhythmia or ischemia (Gheorghiade et al., 2008; Carubelli et al., 2020). However, istaroxime has a plasma half-life of less than 1 hour because of extensive hepatic metabolism to a molecule named PST3093 (Gheorghiade

et al., 2008; Carubelli et al., 2020); this restricts istaroxime usage to acute intravenous therapy.

The present work aims to investigate whether PST3093 may, on its own, be endowed with pharmacological activity. To this end, PST3093 has been synthesized and compared with istaroxime and digoxin (as reference compounds) in experimental setups at different levels of biologic organization and in the context of disease-induced dysfunction.

The data reported here indicate that PST3093 shows a longer half-life in human circulation compared with parent drug; it stimulates SERCA2a activity, but, at variance with istaroxime, it does not inhibit the Na^+/K^+ ATPase. This pharmacodynamic profile translates to positive inotropy and lusitropy in an in vivo disease model characterized by SERCA2a downregulation. Therefore, PST3093 qualifies as a “pure” SERCA2a activator, able to improve cardiac mechanical performance in vivo.

Materials and Methods

This study aims to a comprehensive characterization of PST3093 (versus istaroxime, its parent compound) as an ino-lusitropic agent to be used chronically in the treatment of HF. The evaluations performed and their scope are summarized in Table 1. Further detail on methods is given in the Supplemental Materials.

The animal study protocols were approved by the Institutional Review Board of Milano Bicocca (29C09.26 and 29C09.N.YRR protocol codes approved on January 2021 and June 2018, respectively) and Chang Gung (CGU107-068 protocol code approved on June 2018) Universities in accordance with the Guide for the Care and Use of Laboratory Animals as adopted and promulgated by the US National Institutes of Health.

Disease Model

Streptozotocin (STZ)-induced diabetes was selected as a pathologic model because of its association with reduced SERCA2a function (Torre et al., 2022) and relevance to diastolic dysfunction (Valero-Muñoz et al., 2017), for which a lusitropic action may be more relevant. Diabetes was induced in Sprague-Dawley male rats (150–175 g) by a single STZ (50 $\text{mg}\cdot\text{kg}^{-1}$) intravenous injection (STZ group). Control (healthy group)

TABLE 1
Synopsis of the studies

Evaluation	Experimental Model	Scope
Pharmacokinetics in humans.	Human blood samples from the clinical HORIZON-HF study on istaroxime (Gheorghiade et al., 2008).	To assess compatibility of pharmacokinetics with chronic usage.
Effects on SERCA2a and Na^+/K^+ ATPase activities in cell-free preparations (enzymatic assays).	Tissue homogenates/microsomes from: dog kidney (Na^+/K^+ ATPase); rat and guinea pig ventricle (SERCA2a); guinea pig skeletal muscle (SERCA1).	To assess efficacy and selectivity in modulating the ATPase proteins relevant to the ino-lusitropic effect. Demonstration of PLN-SERCA2a interaction as the molecular target.
In vitro effects for ligands potentially accounting for off-target actions.	High-throughput in vitro ligation to a panel of 50 molecular ligands.	To screen for a wide range of interactors potentially involved in off-target effects.
Effects on Na^+/K^+ ATPase current and intracellular Ca^{2+} dynamics in healthy and diseased myocytes.	Ventricular myocytes isolated from healthy and diseased rats with known SERCA2a dysfunction (STZ-diabetic rats).	To assess in isolated cells efficacy in restoring the SR function in diseased cardiac myocytes.
Effects on electrical activity of healthy myocytes.	Ventricular myocytes isolated from guinea pigs, a species with human-like repolarization.	To test for potential off-target effects of proarrhythmic relevance.
Effects on in vivo hemodynamics of diseased hearts.	Healthy and STZ-diabetic rats; echocardiographic evaluation before and during drug infusion.	To assess efficacy in reversing disease-induced hemodynamic abnormalities in vivo.
In vivo acute toxicity.	Healthy mice; evaluation of LD_{50} .	To assess drug toxicity in vivo.

rats received STZ vehicle (citrate buffer). Fasting glycaemia was measured after 1 week, and rats with values $> 290 \text{ mg-dL}^{-1}$ were considered diabetic (Torre et al., 2022). Rats were euthanized by cervical dislocation under anesthesia with ketamine-xylazine ($130\text{--}7.5 \text{ mg-kg}^{-1} \text{ i.p.}$) 9 weeks after STZ injection.

Pharmacokinetics in Humans

Pharmacokinetics (PKs) of istaroxime and its metabolite PST3093 was assessed in 30 HF patients infused for 6 hours with istaroxime at $1.0 \text{ }\mu\text{g/kg}$ per minute (secondary analysis of the HORIZON-HF study, #NCT00616161) (Gheorghiade et al., 2008). Blood samples were taken before, during, and up to 18 hours after starting the infusion. The lowest concentration resolved by the technique was 2.6 ng-mL^{-1} for istaroxime and 2.9 ng-mL^{-1} for PST3093; lower values were considered as zero. PKs parameters were estimated using the dedicated software Kinetica (version 4.4, Thermo Electron Corp., Waltham, Massachusetts). Samples were excluded from the analysis if contamination was suspected or ≥ 2 consecutive samples were missing. The following PKs parameters were estimated: the maximum observed concentration (C_{max}), the time of C_{max} (T_{max}), the elimination half-life time ($T_{0.5}$), and the area under the concentration curve from the start of istaroxime administration to the time of final sampling (AUC_{last}).

SERCA and Na^+/K^+ ATPase Activities in Cell-Free Preparations

Total ATPase activity was assessed by measuring the rate of ^{32}P -ATP release ($\mu\text{mol}\cdot\text{min}^{-1}$) at 37°C .

The inhibitory effect of compounds on Na^+/K^+ ATPase activities was tested, at multiple concentrations, on suspensions of the enzyme $\alpha 1$ isoform from dog kidney by measuring ^{32}P -ATP hydrolysis as previously described (Ferrandi et al., 1996). Na^+/K^+ ATPase activity was identified as the ouabain (1 mM)-sensitive component of total one; compound efficacy was expressed as IC_{50} .

Measurements on SERCA2a activities were performed in whole tissue homogenates (rat) or in cardiac SR-enriched microsomes (guinea pig), including SERCA2a and PLN (Torre et al., 2022). To test for PLN involvement in the effect of compounds, SERCA1 activity was also measured in PLN-free microsomes (from guinea pig skeletal muscle) before and after reconstitution with the PLN₁₋₃₂ inhibitory fragment at a ratio PLN:SERCA of 300:1. The SERCA component, identified as the cyclopiazonic acid ($10 \mu\text{M}$)-sensitive one, was measured at multiple Ca^{2+} concentrations ($100\text{--}2000 \text{ nM}$) as ^{32}P -ATP hydrolysis (Micheletti et al., 2007), and Ca^{2+} dose-response curves were fitted to estimate SERCA V_{max} ($\mu\text{mol}\cdot\text{min}^{-1}\cdot\text{mg}^{-1}$ protein) and Ca^{2+} dissociation constant (K_{dCa} ; nM). Either an increase of V_{max} or a decrease of K_{dCa} (increased Ca^{2+} affinity) stand for enhancement of SERCA function.

Off-Target Actions

To predict potential off-target actions of PST3093, its interaction with a panel of 50 ligands, potentially relevant to off-target effects, was carried out by Eurofins (Taiwan) on crude membrane preparations according to Eurofins described procedures. PST3093 was tested at the concentration of $10 \mu\text{M}$.

Na^+/K^+ ATPase Current and Intracellular Ca^{2+} Dynamics in Healthy and Diseased Myocytes

To ensure stabilization of drug effect, isolated myocytes were analyzed after incubation with PST3093 or vehicle (control) for at least 30 minutes. Difference between means was thus tested by group comparison. The experiments were performed at 35°C .

Na^+/K^+ ATPase current (I_{NaK}) was recorded (V-clamp) in isolated rat left ventricular (LV) myocytes as the holding current at -40 mV under conditions enhancing I_{NaK} and minimizing contamination by other conductances (Rocchetti et al., 2003; Torre et al., 2022). I_{NaK}

inhibition by the compounds was expressed as percent reduction of ouabain (1 mM)-sensitive current; efficacy was expressed as the IC_{50} effect.

Intracellular Ca^{2+} dynamics were evaluated by Ca^{2+} -dependent fluorescence (Fluo4-AM) in isolated LV myocytes and quantified by normalized units (F/F_0). Properties of voltage-induced Ca^{2+} transients (CaT ; amplitude and decay kinetics) and caffeine-induced ones (estimating total SR Ca^{2+} content; Ca_{SR}) were assessed in intact myocytes, field-stimulated at 2 Hz . A caffeine puff was applied 20 seconds (electronic timing) after a V-triggered loading sequence at 2 Hz . Resting Ca^{2+} (Ca_{rest}) was measured just before caffeine application to reflect the equilibrium value of cytosolic Ca^{2+} . In V-clamped myocytes, SR Ca^{2+} uptake rate was evaluated through an “SR loading” voltage protocol, specifically devised to examine the system at multiple levels of SR Ca^{2+} loading and to rule out $\text{Na}^+/\text{Ca}^{2+}$ exchanger (NCX) contribution. Current through L-type Ca^{2+} channel (I_{CaL}) was simultaneously recorded, and the excitation-release (ER) “gain” was calculated as the ratio between CaT amplitude and Ca^{2+} influx through I_{CaL} up to CaT peak (Rocchetti et al., 2005) (protocol in Supplemental Fig. 1).

Electrical Activity in Healthy Myocytes

Action potentials (AP) were recorded by patch clamp (I-clamp) from isolated guinea pig LV myocytes, selected because of the AP similarity to the human one (Odening et al., 2021), under Tyrode superfusion. Action potential duration (APD) at 50% and 90% repolarization (APD_{50} and APD_{90} , respectively) and diastolic potential (E_{diast}) were measured 1) during steady-state pacing at several rates and 2) dynamically upon stepping between two rates (APD_{90} adaptation). During steady-state pacing, short-term APD_{90} variability (STV) was calculated from 20–30 subsequent APD_{90} values according to eq. 1 (Altomare et al., 2015):

$$\text{STV} = \sum (|\text{APD}(n+1) - \text{APD}n|) / [n \text{beats} \times \sqrt{2}] \quad (1)$$

The kinetics of APD_{90} adaptation was quantified by the time constant (τ) of exponential data fitting.

In Vivo Hemodynamics of Diseased Hearts

Healthy and STZ rats were studied by transthoracic echocardiographic under urethane anesthesia ($1.25 \text{ g}\cdot\text{kg}^{-1} \text{ i.p.}$) by means of a Mindray M9 ultrasound machine (Mindray Co, Shen Zhen, China) equipped with a P10-4s phased ultrasound transducer. LV end-diastolic (LVEDD) and end-systolic (LVESD) diameter, posterior wall thickness (PWT) and interventricular septal (IVST) thickness in systole (s) and diastole (d) were measured according to the American Society of Echocardiography guidelines (Lang et al., 2006). The Teichholz equation ($(7/(2.4 + D) \times D^3)$, $D = \text{LVEDD or LVESD}$) was used to calculate LV end-diastolic volume (EDV) and end-systolic volume (ESV). Stroke volume (SV) was calculated as the difference between EDV and ESV. LV ejection fraction (EF) was calculated as SV/EDV and expressed in percent (Tournoux et al., 2011). Fractional shortening (FS) was calculated as $\text{FS} = (\text{LVEDD} - \text{LVESD})/\text{LVEDD}$ and expressed in percent. Transmittal flow velocity was measured (pulsed Doppler) to obtain early- and late-filling velocities (E and A waves) and E-wave deceleration time (DT). DT was also normalized to E-wave amplitude (DT/E ratio). Peak myocardial systolic (s') and diastolic (e' and a') tissue velocities were measured at the mitral annulus by tissue Doppler imaging. Two-dimensional LV mass and its relative index to body weight were estimated in healthy and STZ rats.

PST3093 was intravenously infused at $0.22 \text{ mg}\cdot\text{kg}^{-1}$ ($0.16 \text{ ml}\cdot\text{min}^{-1}$); echocardiographic parameters were measured before and at 15 and 30 minutes during the infusion. Istaroxime ($0.22 \text{ mg}\cdot\text{kg}^{-1}$) and digoxin ($0.11 \text{ mg}\cdot\text{kg}^{-1}$), both infused for 15 minutes, were used as comparators. A previous study in the same setting demonstrated that neither urethane anesthesia nor the infusion volumes per se affected echocardiographic parameters (Torre et al., 2022).

In Vivo Acute Toxicity

Acute toxicity of PST3093 was preliminarily evaluated in male albino Swiss CD-1 mice by identifying the LD₅₀ (mg·kg⁻¹ body weight) at 24 hours after intravenous injection. PST3093 was dissolved in DMSO and injected at 50, 100, 200, and 250 mg·kg⁻¹ (4 animals for each group). Higher PST3093 dose levels were not tested due to the solubility limit of the compound; control animals received the vehicle only (DMSO).

Acute toxicity of istaroxime in male CD-1 mice was also evaluated for comparison by testing intravenous dose levels of 15, 22, 27, and 33 mg·kg⁻¹ (5 animals for each group). Control animals received the vehicle only (saline).

Statistical Analysis

Individual means were compared by paired or unpaired *t* test; multiple means were compared by one- or two-way ANOVA for repeated measurements (RM) plus post hoc Tukey's multiple comparisons. Drug-induced changes in overall curve steepness were defined according to significance of the "factor X group" interaction. Data are reported as mean ± S.E.M.; *P* < 0.05 defined statistical significance of differences in all comparisons; NS, not significant. Number of animals (*N*) and/or cells (*n*) are shown in each figure legend.

Chemicals

Istaroxime {PST2744: [E,Z]-3-[(2-aminoethoxy)imino]-androstane-6,17-dione hydrochloride} and its metabolite PST3093 {(E,Z)-[(6-β-hydroxy-17-oxoandrostan-3-ylidene)amino]oxyacetic acid} were synthesized and produced at Prassis Research Institute and Sigma-Tau Pharmaceutical Company and then by CVie Therapeutics Limited and WindTree Therapeutics. The batch of PST3093 used for in vitro and in vivo studies was a 1:1 mixture of oxime E:Z isomers. It was synthesized according to standard procedures, characterized by NMR spectroscopy, and its purity (about 95%) was assessed by high-performance liquid chromatography (HPLC) (Supplemental Fig. 2). Digoxin was purchased from Sigma-Aldrich.

Results

Chemical Structure of PST3093

PST3093 is the final metabolite of istaroxime (Gheorghiadu et al., 2008); its chemical structure is shown in Fig. 1A. Compared with istaroxime, PST3093 retains the oxime moiety at position 3 with the amino-chain oxidized into a carboxylic chain, whereas the 6-keto group of istaroxime is stereo selectively reduced to a 6β-hydroxyl group.

Pharmacokinetics

Fig. 1B shows istaroxime and PST3093 plasma levels over a 6-hour istaroxime infusion at 1 μg·kg⁻¹·min⁻¹ and up to 12 hours after discontinuation of infusion in HF patients (Gheorghiadu et al., 2008). All patients showed measurable istaroxime levels until 10 minutes after stopping the infusion; drug levels decreased rapidly thereafter, and just one patient had a quantifiable istaroxime level 2 hours after the end of the infusion. PST3093 plasma levels increased with a lag from the start of istaroxime infusion (as expected for a metabolite) being detectable in all patients from 1 hour after the start of infusion. Plasma PST3093 levels remained detectable long after discontinuation of the infusion, up to the last sample at 12 hours after wash out. The data suggest that, if istaroxime infusion had continued beyond 6 hours, the metabolite would have accumulated further.

In quantitative terms, PST3093 had a T_{0.5} of about 9 hours, i.e., substantially longer than that of istaroxime (less than 1

hour), leading to a huge enhancement of the AUC_{last} index for PST3093; although the C_{max} of PST3093 was similar to istaroxime one at this infusion rate, the T_{max} was longer for PST3093 in comparison with istaroxime (Fig. 1C).

Effect of PST3093 on Na⁺/K⁺ ATPase

Istaroxime and PST3093 effects on Na⁺/K⁺ ATPase activity were tested in a range of concentrations from 10⁻⁹ to 10⁻⁴ M (Fig. 2A). Na⁺/K⁺ ATPase from dog kidney had a specific baseline activity of 14 μmol·min⁻¹·mg⁻¹ protein. The reference compound istaroxime inhibited Na⁺/K⁺ ATPase activity with IC₅₀ of 0.14 ± 0.02 μM in dog kidney (Fig. 2A), which corresponds to a higher affinity as compared with that observed in rat renal preparations [IC₅₀ of 55 ± 19 μM from Torre et al. (2022)]. PST3093 did not inhibit the Na⁺/K⁺ ATPase activity up to 100 μM, the maximal tested concentration (Fig. 2A).

PST3093 effects on I_{NaK} were further evaluated in rat LV myocytes in comparison with istaroxime (Fig. 2B). The estimated IC₅₀ for I_{NaK} inhibition by istaroxime was 32 ± 4 μM [from Torre et al. (2022)]; for PST3093, a barely detectable inhibition (9.2 ± 1.1%) was observed at the limit concentration for solubility (100 μM), an effect that can be considered insignificant.

Effect of PST3093 on SERCA ATPase Activity

Effects on SERCA2a Activity in Normal and Diseased Myocardial Preparations. In STZ rat preparations (*N* = 30), baseline SERCA2a V_{max} was lower (by -27%) than in healthy ones (*N* = 29) (0.199 ± 0.01 versus 0.272 ± 0.01 μmol·min⁻¹·mg⁻¹ protein, *P* < 0.05), with no difference in K_dCa (448 ± 35 versus 393 ± 22 nM, NS), similar to what was reported recently in the same setting (Torre et al., 2022). As also reported previously (Ferrandi et al., 2013), the response of enzyme kinetics parameters to modulation was species specific: whereas in rat preparations, both PST3093 and istaroxime (Fig. 3) increased V_{max}, in guinea pig ones the compounds decreased K_dCa instead (Supplemental Table 1).

Over the whole range of concentration tested (0.1–1 μM), PST3093 and istaroxime failed to affect ATPase Ca²⁺ dependency in healthy rat preparations (Fig. 3, A and C) but similarly increased V_{max} in STZ ones (e.g., +22% and +20%, respectively, at 300 nM) with thresholds at 100 nM and 300 nM for PST3093 and istaroxime, respectively (Fig. 3, B and D); SERCA2a K_dCa in rat preparations was affected by neither istaroxime nor PST3093. Thus, PST3093 and istaroxime displayed similar potency in ameliorating disease-induced depression of SERCA2a ATPase activity.

PST3093 and istaroxime effect was also detected in preparations from normal guinea pig hearts, where they both reduced the SERCA2a K_dCa value by about 20% at 100 nM (Supplemental Table 1).

To summarize, PST3093 and istaroxime equally stimulated SERCA2a ATPase activity in preparations including PLN. Regardless of the kinetic parameter affected, a stimulatory effect was present in healthy guinea pig microsomes and in rat homogenates from the STZ disease model.

Dependency of SERCA Stimulation on PLN. In a range of concentrations from 30 to 1000 nM, PST3093 and istaroxime failed to affect SERCA1 activity in the absence of PLN in skeletal muscle preparations (Fig. 4, A and C). Reconstitution with the PLN₁₋₃₂ fragment markedly reduced SERCA1 affinity

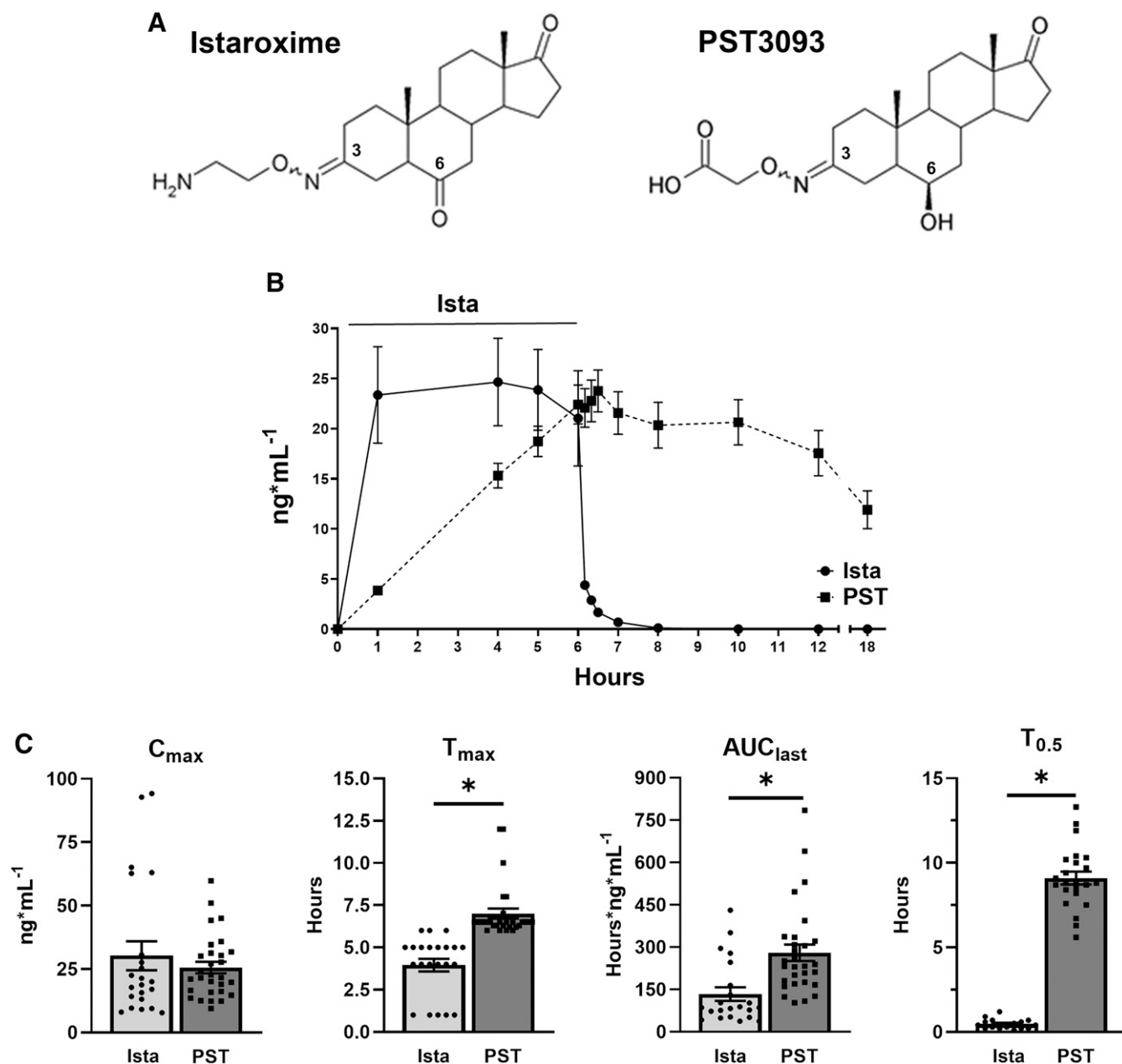


Fig. 1. The chemical structure of istaroxime and its metabolite PST3093 (A) and PKs in humans (B and C). (A) The main metabolic pathways of istaroxime are reduction of the carbonyl in position 6 catalyzed by carbonyl reductases and oxidative deamination of the primary amino group catalyzed by monoamine oxidases or tissue-bound semicarbazide-sensitive amine oxidase. (B) Istaroxime ($N = 22$) and PST3093 ($N = 29$) plasma levels evaluated over 6 hours of istaroxime infusion in HF patients at 1 $\mu\text{g/kg}$ per minute and up to 12 hours after discontinuation of infusion (from HORIZON-HF study, #NCT00616161). (C) Statistics of C_{max} , T_{max} , AUC_{last} , and $T_{0.5}$; * $P < 0.05$ versus istaroxime (unpaired t test). Data are the mean \pm S.E.M. ista, istaroxime; PST, PST3093.

for Ca^{2+} ($K_d\text{Ca}$ increased by 23%–26%) (Fig. 4, B and D). Under this condition, both PST3093 (Fig. 4B) and istaroxime (Fig. 4D) dose-dependently reversed PLN-induced shift in $K_d\text{Ca}$ with an EC_{50} of 39 nM and 40 nM, respectively.

PST3093 Interaction with Targets other than SERCA

The targets panel (50 items) included membrane receptors, key enzymes, ion channels, and transporters relevant to potential off-target cardiac and extracardiac effects (list in Supplemental Table 2); PST3093 was tested at the concentration of 10 μM . None among the 50 items met criteria for significance of interaction.

Thus, at least for the ligands shown in Supplemental Table 2, no off-target action of PST3093 is expected.

Effects of PST3093 on Intracellular Ca^{2+} Dynamics in Cardiac Myocytes

Global Effects in Field Stimulated Myocytes. Ca^{2+} dynamics were analyzed in field-stimulated (2 Hz, Fig. 5) rat LV myocytes isolated from healthy or STZ rats.

STZ myocytes had a lower Ca_{SR} and a slower CaT decay than healthy ones; however, CaT amplitude remained unchanged. These changes are compatible with reduced SERCA2a

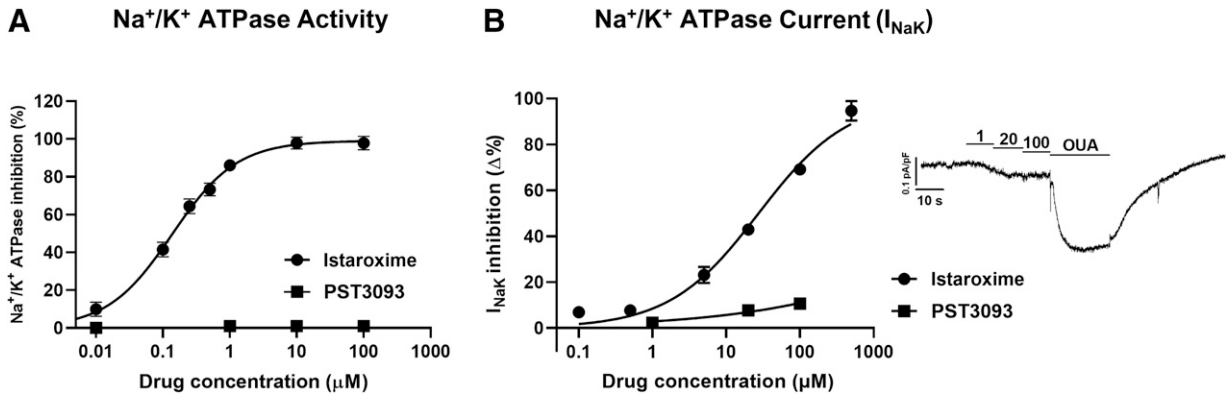


Fig. 2. Modulation of Na⁺/K⁺ ATPase activity. (A) Inhibition of Na⁺/K⁺ ATPase activity by istaroxime and PST3093 in dog renal preparations ($N = 3$). (B) Concentration-response curves for I_{NaK} inhibition by PST3093 ($n = 15$) and istaroxime (modified from Torre et al. (2022); this work is available under a CC-BY-NC license) in rat LV myocytes; I_{NaK} recording under increasing concentrations of PST3093 and finally to ouabain (OUA as reference) is shown on the right. Data are the mean \pm S.E.M.

function, possibly compensated by APD prolongation, known to increase cell Ca²⁺ content (Torre et al., 2022). Whereas in healthy myocytes, 1 μM PST3093 failed to affect any of the Ca²⁺ dynamics parameters, in STZ myocytes PST3093 reduced the quiescence Ca²⁺ (Ca_{rest}) prior to caffeine application and partially restored Ca_{SR} and CaT decay. Moreover, PST3093 restored in STZ myocytes the distribution of Ca_{SR} values peculiar of healthy ones. Comparable results have been obtained with istaroxime at a concentration marginally affecting Na⁺/K⁺ ATPase (Torre et al., 2022). Taken together, this observation suggests that PST3093 improved Ca²⁺ sequestration into the SR during the post-train quiescence period.

Effects on SR Ca²⁺ Uptake Function under NCX Inhibition. STZ-induced changes in repolarization affect Ca²⁺ handling in a direction masking SERCA2a downregulation (Torre et al., 2022). Thus, the “SR loading” protocol (see *Methods* and Supplemental Fig. 1) was performed under V-clamp and used to assess SR Ca²⁺ uptake under conditions emphasizing SERCA2a role (NCX inhibition). In STZ myocytes, as compared with healthy ones, SR reloading was significantly depressed (both in terms of CaT amplitude and ER gain), and CaT decay was slower at all timepoints during reloading (Fig. 6A). These changes are compatible with depressed SERCA2a function (Torre et al., 2022). PST3093 (1 μM) was

SERCA2a ATPase Activity

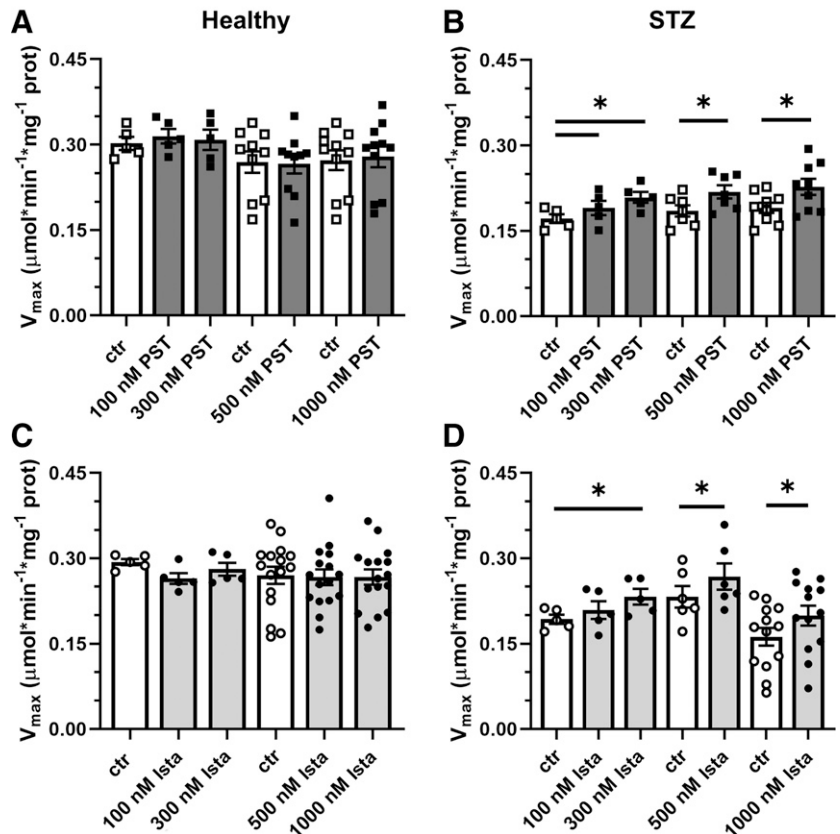


Fig. 3. Modulation of SERCA2a ATPase activity in healthy and diseased (STZ) preparations. Effect of PST3093 ($N = 5-11$) (A and B) and istaroxime ($N = 5-16$) (C and D) on SERCA2a V_{max} estimated from Ca²⁺-dose response curves in cardiac homogenates from healthy and diabetic (STZ) rats. Internal controls (ctr) are provided. Data are the mean \pm S.E.M. * $P < 0.05$ versus ctr (RM one-way ANOVA plus post hoc Tukey's multiple comparisons test or paired t test).

SERCA1 ATPase Activity

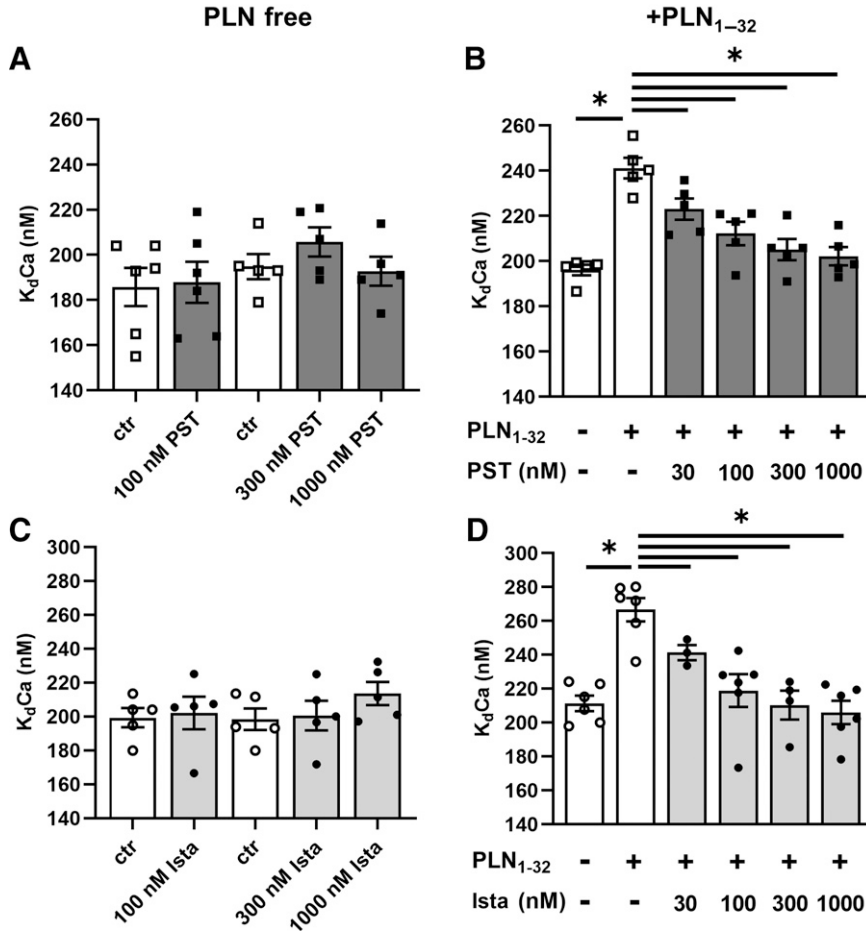


Fig. 4. Modulation of SERCA1 ATPase activity. Concentration dependency of PST3093 and istaroxime modulation of SERCA1 K_dCa in guinea pig skeletal muscle microsomes containing SERCA1 alone (A and C) ($N = 5-6$) and after reconstitution with the PLN₁₋₃₂ fragment (B and D) ($N = 5-6$). Data are the mean \pm S.E.M. * $P < 0.05$ (RM or mixed-model one-way ANOVA plus post hoc Tukey's multiple comparisons).

tested in STZ myocytes (Fig. 6B), where it sharply accelerated CaT decay, restoring the profile observed in healthy myocytes. Albeit less evident, drug-induced changes in CaT and ER gain pointed in the same direction. Comparable results have been obtained with istaroxime at a concentration marginally affecting Na^+/K^+ ATPase (Torre et al., 2022).

Overall, PST3093 restored SR function in diseased myocytes, i.e., the context of the pathologic cellular environment, most likely through SERCA2a enhancement.

Effects of PST3093 on Cellular Electrical Activity

To assess the electrophysiological safety of PST3093, its effects on AP of LV myocytes were investigated. Guinea pig myocytes were used instead of rat ones because their AP is closer to the human one.

PST3093 (100 nM) marginally reduced APD_{50} at all pacing rates, leaving the other AP parameters unchanged (Fig. 7, A and B). Notably, also APD rate dependency at steady-state and the kinetics of APD adaptation following a step change in rate were unaffected by the agent (Fig. 7C). STV of APD_{90} , a reporter of repolarization stability, was also unaffected by PST3093 at all pacing rates (Fig. 7, D and E). Except for the absence of APD_{50} reduction, similar results were obtained with PST3093 at 1 μ M (Supplemental Fig. 3).

The paucity of PST3093 effects on the AP is consistent with the absence of hits in the analysis of PST3093 interaction (up to 10 μ M) with molecular targets other than SERCA2a, among them ion channels and transporters (Supplemental Table 2).

In Vivo Acute Toxicity in Mice

In vivo toxicity after intravenous injection was investigated in mice for PST3093 and istaroxime. PST3093 was well tolerated and did not cause death up to 250 mg/kg. The LD_{50} was not calculated since no deaths occurred at the maximal usable dose (limited by solubility). The LD_{50} for istaroxime was 23.06 mg/kg. The main signs of toxicity were prostration, gasping, and convulsions. In most of the animals, death occurred within 5 minutes after istaroxime administration. Postmortem examination revealed pulmonary edema and/or hemorrhages and generalized organ congestion. No remarkable alterations were found in the surviving animals.

Therefore, when intravenously administered, PST3093 was far less toxic than istaroxime, a result ascribable to its lack of effects on the Na^+/K^+ ATPase.

Modulation of Cardiac Function in Vivo in Rats with Diabetic Cardiomyopathy

In vivo cardiac function was evaluated by echocardiography. In light of the uncertainty inherent to the mechanistic interpretation

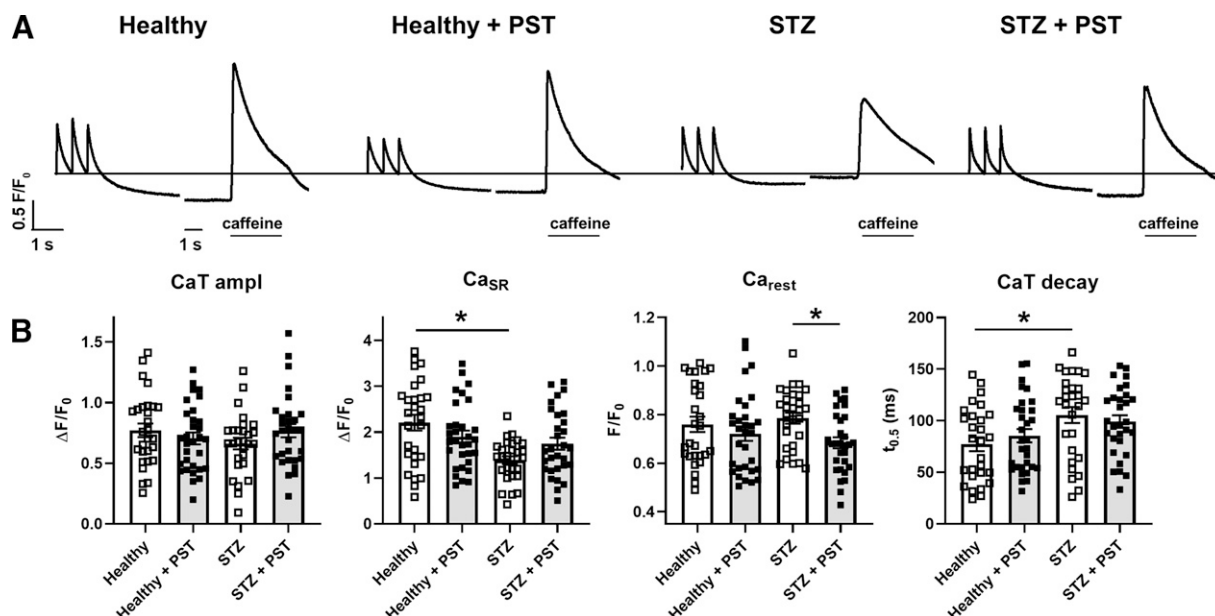


Fig. 5. Modulation of intracellular Ca²⁺ handling in field-stimulated myocytes from healthy and diseased (STZ) hearts. (A) Representative recordings of CaT triggered by steady-state electrical stimulation at 2 Hz in intact cells, followed after 20 seconds by caffeine-induced Ca²⁺ release measuring CaSR. PST3093 (1 μ M) was tested in normal (healthy) and STZ myocytes. (B) Statistics for CaT amplitude (ampl), CaSR, Ca_{rest}, and time for 50% CaT decay ($t_{0.5}$). CTR $N = 3$ ($n = 28$ without PST3093; $n = 31$ with PST3093), STZ $N = 4$ ($n = 28$ without PST3093; $n = 30$ with PST3093). * $P < 0.05$ (one-way ANOVA plus post hoc Tukey's multiple comparisons).

of drug effect on individual echo indexes, this set of experiments was designed to test whether PST3093 was able to reverse the derangements peculiar of the STZ disease model. To this end, the STZ model had to be first characterized.

Features of the Disease Model. Fasting hyperglycemia, polydipsia, polyuria, and polyphagia ensued 1 week after STZ injection; none of these symptoms was observed

in healthy rats. Eight weeks after STZ, total body weight was substantially lower in STZ rats; LV mass (by echo) was reduced in absolute value but, when normalized to body weight, was not significantly different in STZ rats (Supplemental Table 3). The STZ model was largely characterized in a previous work of ours (Torre et al., 2022).

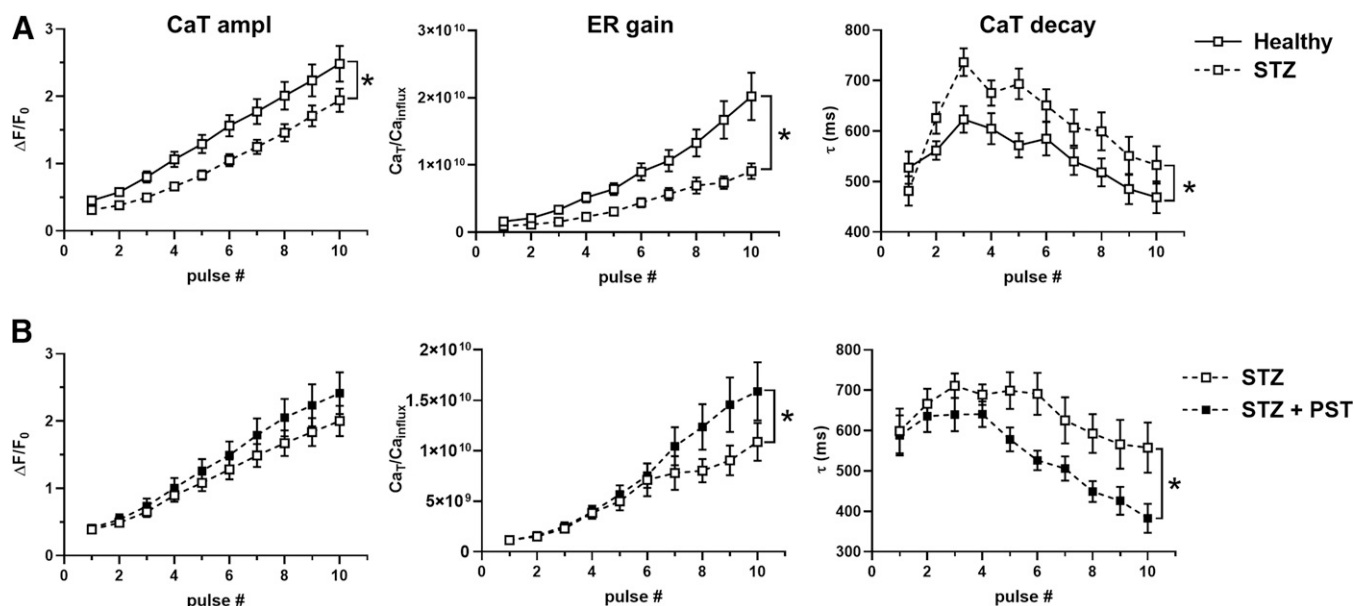


Fig. 6. Modulation of SR Ca²⁺ uptake under NCX inhibition in V-clamped myocytes from STZ hearts. (A) Disease (STZ) effect on SR Ca²⁺ loading in patch-clamped myocytes. SR Ca²⁺ loading by a train of V-clamp pulses was initiated after caffeine-induced SR depletion; NCX was blocked by Na⁺ substitution to identify SERCA2a-specific effects (see *Methods* and Supplemental Fig. 1); myocytes from healthy ($N = 9$; $n = 32$) and diseased hearts ($N = 6$; $n = 31$) are compared. (B) PST3093 effect in STZ myocytes ($N = 4$; without PST3093 $n = 18$, with PST3093 $n = 19$). Panels from left to right: CaT amplitude, ER gain (the ratio between CaT amplitude and Ca²⁺ influx through I_{CaL}), and τ of CaT decay. * $P < 0.05$ for the "interaction factor" in RM two-way ANOVA, indicating a different steepness of curves.

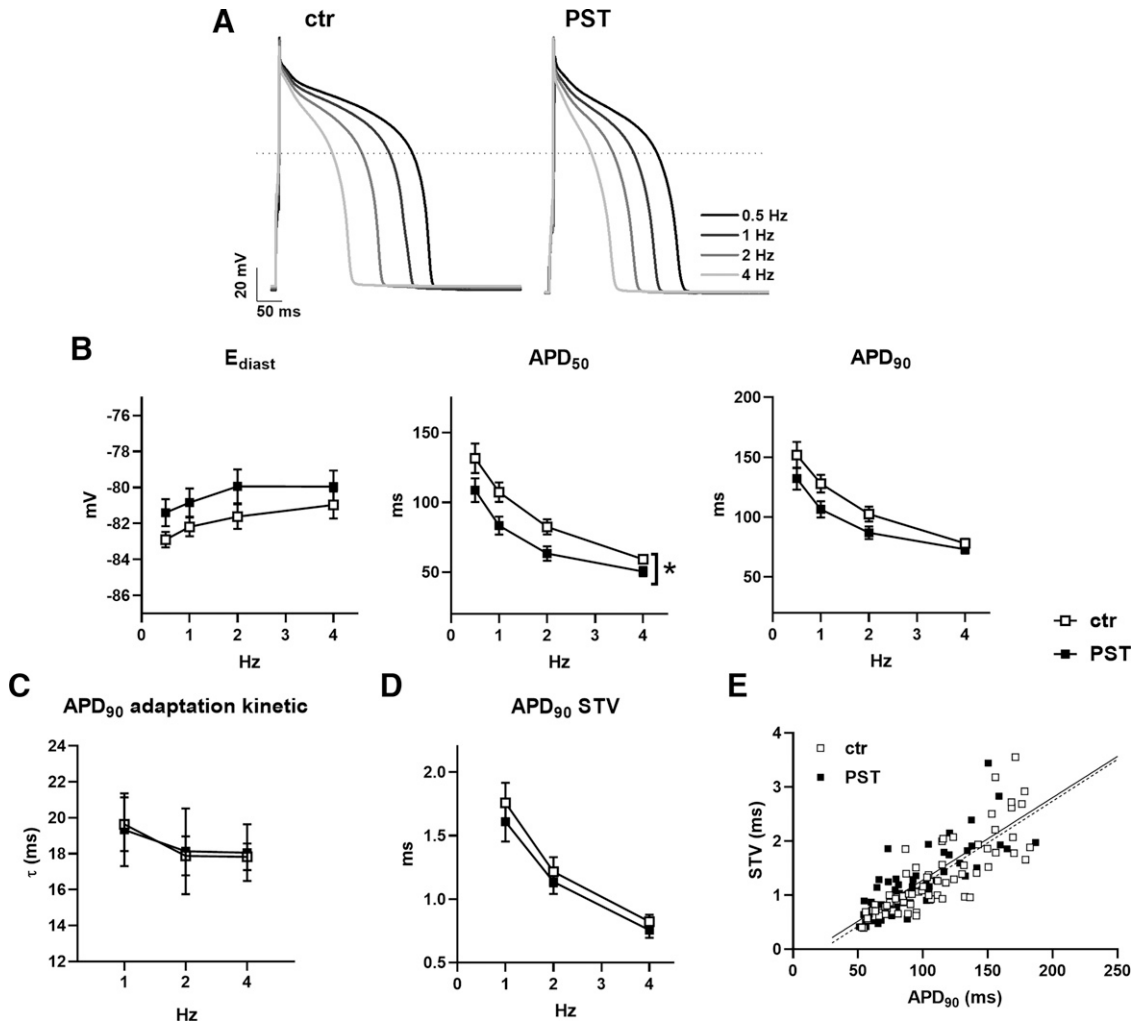


Fig. 7. Modulation of electrical activity in guinea pig myocytes. The effect of 100 nM PST3093 was tested on AP parameters and their steady-state rate dependency in guinea pig myocytes ($N = 5$). (A) representative APs recorded at 0.5, 1, 2, and 4 Hz in control (left) and with 100 nM PST3093 (right). (B) Effect on the rate dependency of diastolic potential (E_{diast}) and AP duration (APD_{50} , APD_{90}) ($n \geq 24$ without PST3093; $n \geq 22$ with PST3093). (C) Effect on the τ of APD_{90} adaptation following a step change in rate ($n \geq 22$ without PST3093; $n \geq 16$ with PST3093). (D) Effect on the rate dependency of APD_{90} STV ($n \geq 24$ without PST3093; $n \geq 20$ with PST3093). (E) Effect on the correlation between STV of APD_{90} and APD_{90} values; data from 1, 2, and 4 Hz were pooled. $*P < 0.05$ for the “interaction factor” of RM two-way ANOVA. The effect of PST3093 at a higher concentration (1 μ M) is reported in Supplemental Fig. 3.

In this study, a comprehensive echocardiographic analysis of STZ rats in comparison with healthy ones was performed. Figure 8 compares some echo indexes in STZ versus healthy rats; Supplemental Table 4 lists all the measured echo parameters in the two groups. Heart rate (HR) was lower in STZ rats (-20% ; $P < 0.05$), and SV was unchanged; nonetheless, differences in cardiac output (CO) between the two groups did not achieve significance. *Systolic indexes:* in STZ rats, LVESD was larger, and the EF was reduced; FS and systolic tissue velocity (s') were depressed. *Diastolic indexes:* in STZ rats, LVEDD tended to be larger; peak E-wave velocity (E) was slightly smaller, and A-wave velocity (A) was unchanged (E/A unchanged); E-wave DT was unchanged in absolute, but the DT/E ratio was increased. Changes in early (e') and late (a') diastolic tissue velocities paralleled those in E and A waves; therefore, the e'/a' and E/e' ratios did not differ between STZ and healthy rats.

To summarize, in STZ rat, echocardiographic abnormalities were rather subtle; nonetheless, 11 out of 21 indexes were

significantly affected, indicating derangements in both systolic and diastolic function.

Drug Effects in the Disease Model. The in vivo acute effect of PST3093 ($0.22 \text{ mg} \cdot \text{kg}^{-1} \cdot \text{min}^{-1}$) on echo indexes of STZ rats was investigated at 15 and 30 minutes of infusion (Fig. 9). Data at 15 minutes were also obtained with istaroxime ($0.22 \text{ mg} \cdot \text{kg}^{-1} \cdot \text{min}^{-1}$) and digoxin ($0.11 \text{ mg} \cdot \text{kg}^{-1} \cdot \text{min}^{-1}$) (Table 2). Overall, PST3093 increased SV volume and CO, without changing HR (Fig. 9). *Systolic indexes:* PST3093 tended to decrease LVESD and increased FS, EF, and s' . *Diastolic indexes:* PST3093 increased LVEDD, E, A (at 30 minutes), and e' (E/A and E/e' unchanged, Table 2); DT and DT/E were reduced. PST3093 effect was almost complete at 15 minutes of infusion; only minor increments were observed at 30 minutes (Fig. 9). Collectively, PST3093 improved overall cardiac function, both systolic and diastolic, beyond simple recovery of STZ-induced derangements. As shown in Fig. 9, PST3093 “reversed” STZ-induced changes in 7 out of 11 indexes; moreover, five additional indexes, unaffected by STZ,

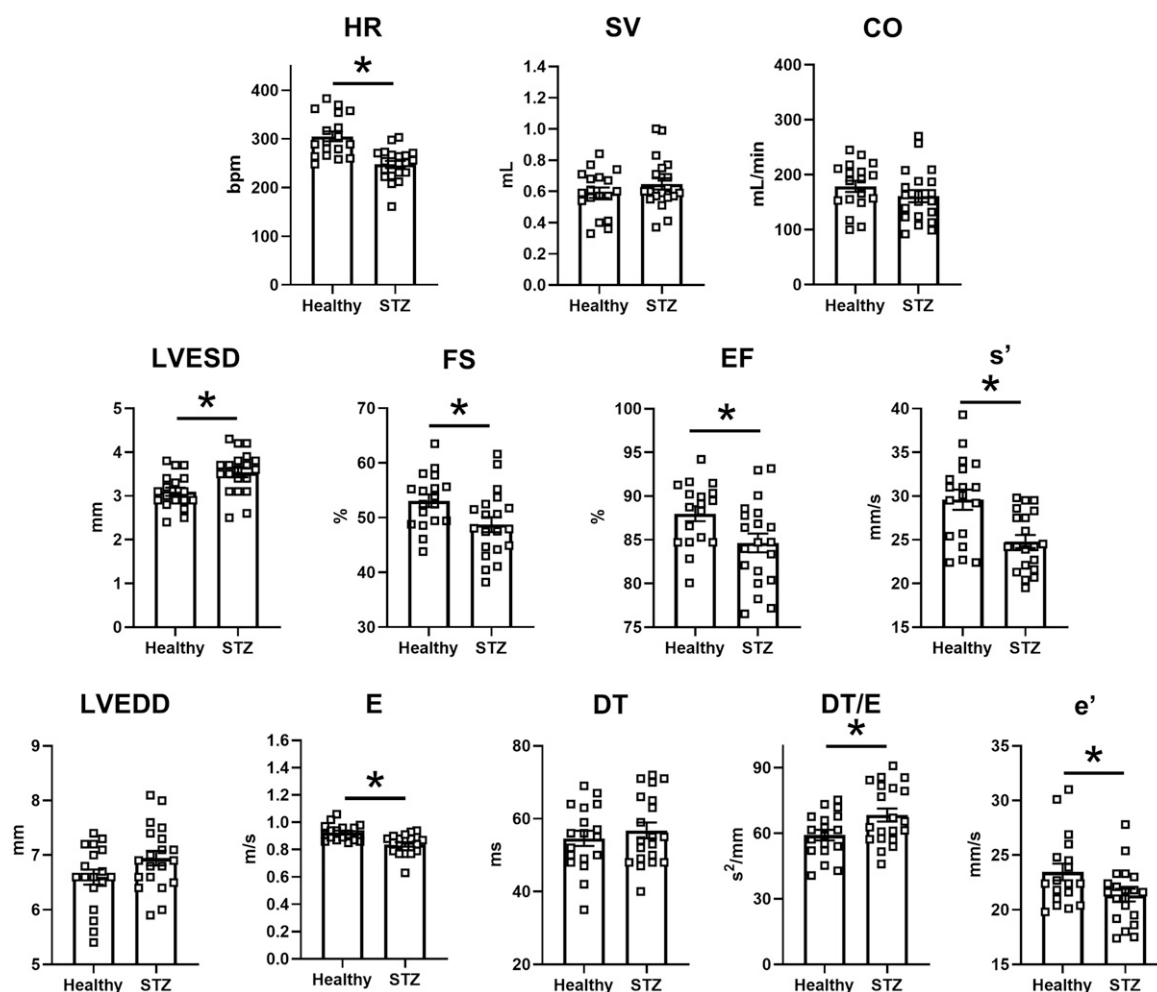


Fig. 8. Disease (STZ) effects on in vivo echocardiographic parameters. Echocardiographic parameters are compared between healthy rats ($N = 18$) and 8 weeks after STZ treatment ($N = 20$). Top row, global function parameters; mid row, systolic function parameters; bottom row, diastolic function parameters: * $P < 0.05$ (unpaired t test).

were changed by PST3093 in a direction compatible with positive inotropy/lusitropy (Table 2).

PST3093 effects were only partially shared by istaroxime at the same infusion rate (Table 2). Istaroxime failed to increase SV and systolic indexes (SV, FS, EF, s'); it increased CO, but, at variance with PST3093, this was because HR increased. Similar to PST3093, istaroxime shortened DT and DT/E and increased e', a', and A; however, it did not change E, thus reducing E/e'. Digoxin (Table 2), as expected from its inotropic effect, increased systolic indexes (FS, EF, and s'); however, at variance with PST3093, it did not affect SV or CO. Notably, digoxin also improved diastolic function to some extent: E/A, DT, and DT/E were reduced, and e' was increased.

Discussion

In the present study, we have investigated the effects of the istaroxime metabolite PST3093 at molecular, cellular, and in vivo levels. The interest in this molecule is motivated by 1) the possibility that it may actually contribute to (i.e., be endowed with) the unique mechanism of action and interesting therapeutic profile of istaroxime (inotropy and lusitropy at low proarrhythmic risk, confirmed in phase 2 clinical trials)

(Sabbah et al., 2007; Gheorghiade et al., 2008; Shah et al., 2009; Carubelli et al., 2020) and 2) the possibility that it would afford to test the clinical benefit associated specifically with the rescue of SERCA2a depression, which is widely recognized as the basis for many among HF abnormalities.

PST3093 effect has been tested in three experimental settings with incremental levels of biologic organization, including in vivo measurements from diseased hearts. The consistency of effects across these three sets of experiments confers robustness to the findings.

The results of molecular studies indicate that PST3093 differs from istaroxime because it is devoid of any inhibitory activity on the Na^+/K^+ ATPase while retaining SERCA2a stimulatory action. This identifies PST3093 as a "selective" SERCA2a activator. The results also indicate that, similar to istaroxime (Ferrandi et al., 2013), PST3093 may act by weakening SERCA-PLN interaction. In rat preparations, PST3093 (and istaroxime) increased SERCA2a V_{max} . Although this apparently conflicts with the notion that interference with PLN should decrease the $K_d\text{Ca}$ instead (Brittsan et al., 2003), the same pattern coexisted with evidence, by several independent approaches, of istaroxime antagonism of SERCA2a-PLN interaction (Ferrandi et al., 2013). The reason for this apparent

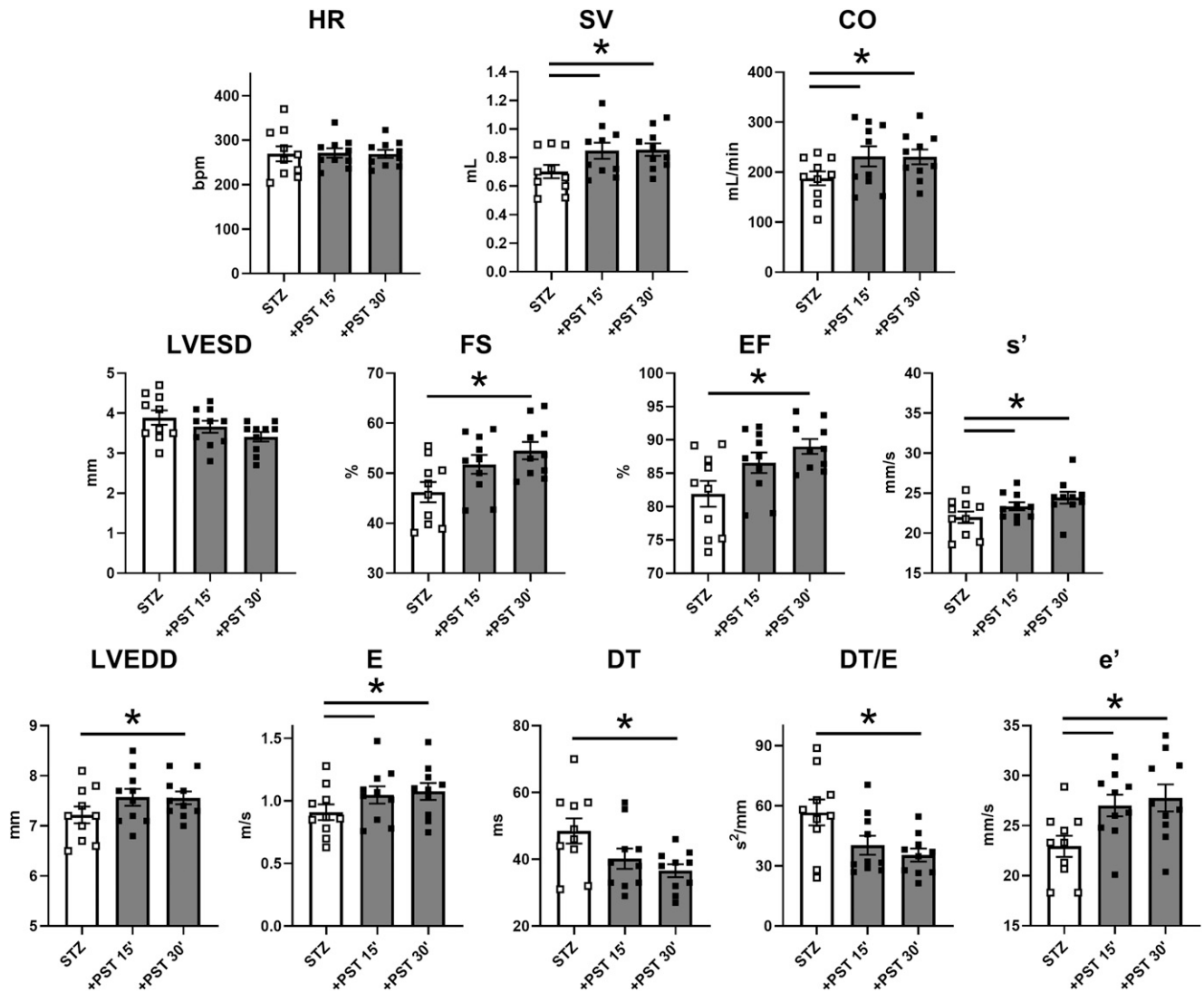


Fig. 9. PST3093 effects on in vivo echocardiographic parameters in diseased (STZ) rats. PST3093 was intravenously infused ($0.22 \text{ mg} \cdot \text{kg}^{-1} \cdot \text{min}^{-1}$) in rats 8 weeks after STZ treatment. Echocardiographic parameters were measured before and at 15 and 30 minutes during drug infusion. Rows and symbols as in Fig. 8; $N = 10$ rats. Data are the mean \pm S.E.M. * $P < 0.05$ (RM one-way ANOVA plus post hoc Tukey's multiple comparisons). Effects of PST3093 on all echocardiographic parameters at 15 minutes of infusion in STZ rats in comparison with istaroxime and digoxin are reported in Table 2.

discrepancy is unclear; the observation that PST3093 effect on SR Ca^{2+} uptake was present in rat cardiac myocytes (i.e., at physiologic Ca^{2+} concentrations) suggests that it may reside in specificities of the microsomal preparation.

Investigations in intact ventricular myocytes confirm a negligible effect of PST3093 on Na^+/K^+ pump function. Furthermore, PST3093 abolished STZ-induced intracellular Ca^{2+} abnormalities likely dependent on SERCA2a downregulation. Although PST3093 clearly affected several Ca^{2+} cycling parameters under V-clamp conditions (Fig. 6), its effects in field-stimulated cells were apparently small (Fig. 5). As we have previously shown in this experimental model (Torre et al., 2022), evaluation of Ca^{2+} handling without controlling membrane potential (field stimulation) and without disabling competing mechanisms (NCX) may be unsuitable to detect SERCA2a activation. This is why we also performed experiments under V-clamp and with disabled NCX function, shown in Fig. 6. Field-stimulation experiments are nonetheless informative because they better represent drug effects at

the cell level under “physiological” conditions. In particular, the reduction in Ca_{rest} indicates that PST3093 allows the other Ca^{2+} cycling parameters to be preserved (or even showing a trend to improve) at a lower cytosolic Ca^{2+} level. Considering that all Ca^{2+} homeostatic mechanisms are in place in this setting, this is precisely what should be expected from pure SERCA2a activation (Alemani et al., 2011; Zaza and Rocchetti, 2015), i.e., improved subcellular Ca^{2+} compartmentalization. That this apparently small change in myocyte physiology has an impact on in vivo cardiac performance is shown by the in vivo echo measurements (Fig. 9).

The present in vivo studies were conducted by echocardiography in a disease model characterized by impairment of SERCA2a function (Choi et al., 2002; Torre et al., 2022). In this model, PST3093 infusion improved overall cardiac performance (SV and CO); both systolic and diastolic indexes were positively affected by the agent. Mechanistic interpretation of echocardiographic indexes is often ambiguous. For instance, both DT prolongation and shortening have been associated

TABLE 2

Effects of PST3093 (0.22 mg.kg⁻¹.min⁻¹), istaroxime (0.22 mg.kg⁻¹.min⁻¹), and digoxin (0.11 mg.kg⁻¹.min⁻¹) on echo indexes of STZ rats at 15 minutes of infusion
Data are the mean ± S.E.M.

Echo Parameters		Istaroxime		PST3093		Digoxin	
		Before	At 15 Min	Before	At 15 Min	Before	At 15 Min
Morphometric Parameters	IVSTd (mm)	1.91 ± 0.09	1.97 ± 0.16	1.89 ± 0.09	1.86 ± 0.11	1.79 ± 0.07	1.81 ± 0.04
	PWTd (mm)	1.6 ± 0.07	1.68 ± 0.09	1.46 ± 0.05	1.47 ± 0.07	1.71 ± 0.08	1.66 ± 0.1
	LVEDD (mm)	7.25 ± 0.15	7.1 ± 0.2	7.22 ± 0.17	7.57 ± 0.17	6.76 ± 0.15	6.67 ± 0.15
	IVSTs (mm)	2.4 ± 0.1	2.45 ± 0.12	2.16 ± 0.11	2.31 ± 0.13	2.25 ± 0.14	2.31 ± 0.1
	PWTs (mm)	2.33 ± 0.16	2.42 ± 0.15	2.43 ± 0.12	2.62 ± 0.14	2.47 ± 0.16	2.68 ± 0.14
	LVEDS (mm)	3.82 ± 0.21	3.8 ± 0.2	3.89 ± 0.18	3.66 ± 0.15	3.53 ± 0.17	3.14 ± 0.14 ^a
Systolic Parameters	FS (%)	47.21 ± 2.4	46.72 ± 2.1	46.2 ± 2.02	51.8 ± 1.89 ^a	47.62 ± 1.9	53.09 ± 1.8 ^a
	s' (mm/s)	23.37 ± 0.9	23.05 ± 0.7	22.0 ± 0.72	23.4 ± 0.5 ^a	23.5 ± 0.9	26 ± 1.5 ^a
	EF (%)	83 ± 2	82 ± 62	82 ± 1.9	87 ± 1.5 ^a	84 ± 1.5	88 ± 1.3 ^a
Diastolic Parameters	E (mm/s)	0.91 ± 0.04	0.94 ± 0.04	0.91 ± 0.06	1.05 ± 0.07 ^a	0.831 ± 0.03	0.924 ± 0.06
	A (mm/s)	0.66 ± 0.04	0.78 ± 0.05 ^a	0.79 ± 0.08	0.87 ± 0.07	0.59 ± 0.05	0.79 ± 0.05 ^a
	E/A	1.39 ± 0.06	1.22 ± 0.08	1.18 ± 0.05	1.22 ± 0.04	1.48 ± 0.11	1.2 ± 0.06 ^a
	DT (ms)	46.62 ± 4.1	34.12 ± 2.5 ^a	48.5 ± 3.8	40.2 ± 3.0	53.4 ± 3.8	44.1 ± 3.2 ^a
	DT/E	51.91 ± 4.9	36.66 ± 3.3 ^a	56.7 ± 6.5	40.39 ± 4.8 ^a	65.21 ± 5.3	50.18 ± 5.4 ^a
	E/DT	21.28 ± 3.2	28.98 ± 2.8 ^a	20.61 ± 3.0	27.51 ± 2.6 ^a	16.53 ± 1.7	22.66 ± 3.0
	e' (mm/s)	21.23 ± 0.99	24.73 ± 0.61 ^a	22.94 ± 1.0	27.01 ± 1.1 ^a	20.9 ± 0.5	23.8 ± 0.9 ^a
	a' (mm/s)	27.61 ± 1.9	31.35 ± 1.5 ^a	28.72 ± 2.2	31.06 ± 1.5	25.9 ± 1.9	29.8 ± 1.9
	e'/a'	0.78 ± 0.04	0.79 ± 0.03	0.83 ± 0.06	0.88 ± 0.04	0.85 ± 0.06	0.82 ± 0.04
	E/e'	43.6 ± 2.6	38.29 ± 1.6 ^a	39.5 ± 1.7	38.61 ± 1.5	39.64 ± 0.9	38.95 ± 2.3
Cardiac Function	HR (bpm)	266.2 ± 9.8	316.2 ± 7.5 ^a	270 ± 17	271 ± 10	236 ± 12	257 ± 11
	SV (ml)	0.71 ± 0.04	0.67 ± 0.05	0.702 ± 0.05	0.847 ± 0.06 ^a	0.589 ± 0.03	0.601 ± 0.04
	CO (ml/min)	188.8 ± 10.5	211.2 ± 13.2 ^a	187.7 ± 13.7	231.7 ± 20.2 ^a	138.5 ± 11.2	155.6 ± 14.4
	N	8	8	10	10	10	10

^aP < 0.05 versus before drug infusion (paired *t* test).

with deterioration of diastolic function (Eren et al., 2004; Sabbah et al., 2007). These puzzling observations can be interpreted by considering the contribution to DT of opposing factors, each prevailing in a specific condition (Mossahebi et al., 2015). At any rate, whenever HF was associated with DT shortening, istaroxime (having PST3093 as a metabolite) prolonged it (Sabbah et al., 2007; Shah et al., 2009). A further difficulty may arise from the expectation that ino-lusitropy may increase atrial contraction (A amplitude) and ventricular relaxation (E amplitude) at the same time, thus conceivably making their ratio (E/A) unable to detect drug effects on diastolic function. A similar consideration applies to the E/e' index. An approach to the interpretation of drug effects, independent of mechanistic models, is to check whether the drug counters disease-induced abnormalities. In the case of PST3093, this was true for the majority of indexes (7 out of 11), the most notable exception being a small further increase in LVEDD. Although increments in LVEDD are usually associated with deterioration of systolic function, PST3093 tended to decrease LVESD instead. The LVEDD increment was indeed associated with increased SV and EF, to which it likely contributed.

With the exception of guinea pigs, PST3093 efficacy on SERCA2a function in the diseased condition consistently contrasted with the lack of effect in healthy preparations (Figs. 3 and 5). This suggests that SERCA2a function, although not strictly limiting in health, may become so whenever its "reserve" is diminished. This view may not clash with the clear-cut effect of PLN knockout in healthy murine myocytes; indeed, SERCA2a modulation by PST3093 may be, albeit functionally significant, subtler than complete PLN ablation.

Although failing to increase the amplitude of CaT, PST3093 improved echo indexes of systolic function. Mechanisms at two

levels may account for this observation: at the intracellular level, increased compartmentation of Ca²⁺ within the SR may improve the energetic efficiency of Ca²⁺ cycling (Shannon et al., 2001); at the organ level, improved relaxation may increase preload, with its well known impact on systolic force (Shiels and White, 2008). Indeed, normalization of diastolic function in HF patients with preserved EF may restore CO irrespective of changes in the latter (Tobushi et al., 2017). On the other hand, digoxin, whose mechanism of action is purely inotropic, accelerated early relaxation (DT shortening and e' increase). This is consistent with systo-diastolic coupling, i.e., the contribution to early relaxation of elastic restitution (recoil) of systolic force (Burns et al., 2009).

Besides affording inotropy and lusitropy, SERCA2a stimulation may improve intracellular Ca²⁺ compartmentalization, with potential long-term effects on energetic efficiency and biology of cardiac myocytes (Zaza and Rocchetti, 2015).

PST3093 is remarkably less toxic than istaroxime, which, in turn, has a lower proarrhythmic risk as compared with digoxin (Micheletti et al., 2002). We speculate that the low PST3093 toxicity, relative to istaroxime, may be due to its failure to inhibit the Na⁺/K⁺ pump. The absence of interaction with 50 cardiac and noncardiac targets commonly involved in drug toxicity provides at least a first-level evidence of PST3093 suitability as a therapeutic agent.

Limitations. Whereas in the in vivo experiments, PST3093 effects generally achieved a maximum at 30 minutes of infusion, the istaroxime infusion period was limited to 15 minutes. Our previous study (Torre et al., 2022) indicates that a 15-minute infusion is sufficient for modulation of diastolic parameters by istaroxime. This timepoint was selected in the present study to minimize metabolism to PST3093, thus allowing it to differentiate istaroxime's own effect from that of its metabolite.

Nonetheless, istaroxime effects reported here might differ from the steady-state ones described in previous studies (Sabbah et al., 2007; Shah et al., 2009; Carubelli et al., 2020), to which PST3093 (the metabolite) might actually contribute.

Echo parameters are sensitive to changes in blood pressure, which was not directly measured. Nonetheless, previous in vivo studies ruled out the effect of infused isatroxime and, implicitly, of PST3093 on pulmonary and peripheral resistances (Gheorghiade et al., 2008).

Translation of the present in vivo results to human therapy has to consider differences between clinical HF and the STZ rat model, which has specific hemodynamic features (Mihm et al., 2001). However, consistency of the istaroxime effect reported here with that described in HF patients (Carubelli et al., 2020) supports this translation.

Therapeutic Relevance and Perspective. The results of this study identify PST3093 as a prototype “selective” (i.e., devoid of Na^+/K^+ pump inhibition) SERCA2a activator. This may entail significant differences from the already characterized pharmacodynamic profile of istaroxime.

In the case of istaroxime, lack of the proarrhythmic effect [expected from Na^+/K^+ ATPase inhibition (Rocchetti et al., 2005)] is likely due to SERCA2a stimulation. Indeed, the latter may reduce the occurrence of “ Ca^{2+} waves” and the resulting “triggered activity” (Bai et al., 2013; Zaza and Rocchetti, 2015; Fernandez-Tenorio and Niggl, 2018). It is logical to predict that a pure SERCA2a activator may exert substantial antiarrhythmic effects, at least under the common conditions characterized by SR instability (e.g., HF). On the other hand, Na^+/K^+ pump inhibition may contribute to inotropy; thus, at least theoretically, PST3093 should increase systolic force less than istaroxime. The present results argue for a PST3093 effect on global cardiac function, including positive inotropy. Moreover, compared with istaroxime, PST3093 has a much longer half-life that, per se, may also prolong the beneficial hemodynamic effect of istaroxime infusion.

Overall, PST3093 acting as “selective” SERCA2a activator can be considered the prototype of a novel pharmacodynamic class for the ino-lusitropic approach of HF. After more than 50 years from the suggestion of the involvement of a reduced SERCA2a function as a cause of the depressed cardiac function and the increased arrhythmias in HF, we may have the possibility to prove this hypothesis and provide a “causal” and selective therapy for HF patients.

Authorship Contributions

Participated in research design: Peri, Ferrari, Bianchi, Rocchetti, Zaza.
Conducted experiments: Arici, Ferrandi, Barassi, Hsu, Chang.
Performed data analysis: Arici, Ferrandi, Hsu, Torre, Luraghi, Ronchi.

Wrote or contributed to the writing of the manuscript: Rocchetti, Zaza.

References

Alemanni M, Rocchetti M, Re D, and Zaza A (2011) Role and mechanism of subcellular Ca^{2+} distribution in the action of two inotropic agents with different toxicity. *J Mol Cell Cardiol* **50**:910–918.
 Altomare C, Bartolucci C, Sala L, Bernardi J, Mostacciolo G, Rocchetti M, Severi S, and Zaza A (2015) IKr Impact on Repolarization and Its Variability Assessed by Dynamic Clamp. *Circ Arrhythm Electrophysiol* **8**:1265–1275.
 Arai M, Alpert NR, MacLennan DH, Barton P, and Periasamy M (1993) Alterations in sarcoplasmic reticulum gene expression in human heart failure. A possible mechanism for alterations in systolic and diastolic properties of the failing myocardium. *Circ Res* **72**:463–469.
 Bai Y, Jones PP, Guo J, Zhong X, Clark RB, Zhou Q, Wang R, Vallmitjana A, Benitez R, Hove-Madsen L, et al. (2013) Phospholamban knockout breaks arrhythmogenic

Ca^{2+} waves and suppresses catecholaminergic polymorphic ventricular tachycardia in mice. *Circ Res* **113**:517–526.
 Bers DM and Despa S (2006) Cardiac myocytes Ca^{2+} and Na^+ regulation in normal and failing hearts. *J Pharmacol Sci* **100**:315–322. DOI: 10.1254/jphs.cpj06001x.
 Brittsan AG, Ginsburg KS, Chu G, Yatani A, Wolska BM, Schmidt AG, Asahi M, MacLennan DH, Bers DM, and Kranias EG (2003) Chronic SR Ca^{2+} -ATPase inhibition causes adaptive changes in cellular Ca^{2+} transport. *Circ Res* **92**:769–776.
 Burns AT, La Gerche A, Prior DL, and Macisaac AI (2009) Left ventricular untwisting is an important determinant of early diastolic function. *JACC Cardiovasc Imaging* **2**:709–716.
 Carubelli V, Zhang Y, Metra M, Lombardi C, Felker GM, Filippatos G, O'Connor CM, Teerlink JR, Simmons P, Segal R, et al.; Istaroxime ADHF Trial Group (2020) Treatment with 24 hour istaroxime infusion in patients hospitalized for acute heart failure: a randomised, placebo-controlled trial. *Eur J Heart Fail* **22**:1684–1693.
 Choi KM, Zhong Y, Hoit BD, Grupp IL, Hahn H, Dilly KW, Guatimosim S, Lederer WJ, and Matlib MA (2002) Defective intracellular Ca^{2+} signaling contributes to cardiomyopathy in Type 1 diabetic rats. *Am J Physiol Heart Circ Physiol* **283**:H1398–H1408.
 del Monte F, Harding SE, Dec GW, Gwathmey JK, and Hajjar RJ (2002) Targeting phospholamban by gene transfer in human heart failure. *Circulation* **105**:904–907.
 Eren M, Gorgulu S, Uslu N, Celik S, Dagdeviren B, and Tezel T (2004) Relation between aortic stiffness and left ventricular diastolic function in patients with hypertension, diabetes, or both. *Heart* **90**:37–43.
 Fernandez-Tenorio M and Niggl E (2018) Stabilization of Ca^{2+} signaling in cardiac muscle by stimulation of SERCA. *J Mol Cell Cardiol* **119**:87–95.
 Ferrandi M, Barassi P, Tadini-Buoninsegni F, Bartolommei G, Molinari I, Tripodi MG, Reina C, Moncelli MR, Bianchi G, and Ferrari P (2013) Istaroxime stimulates SERCA2a and accelerates calcium cycling in heart failure by relieving phospholamban inhibition. *Br J Pharmacol* **169**:1849–1861.
 Ferrandi M, Tripodi G, Salardi S, Florio M, Modica R, Barassi P, Parenti P, Shainskaya A, Karlish S, Bianchi G, et al. (1996) Renal Na,K-ATPase in genetic hypertension. *Hypertension* **28**:1018–1025.
 Gheorghiade M, Blair JEA, Filippatos GS, Macarie C, Ruzyllo W, Korewicki J, Bubenek-Turconi SI, Ceracchi M, Bianchetti M, Carminati P, et al.; HORIZON-HF Investigators (2008) Hemodynamic, echocardiographic, and neurohormonal effects of istaroxime, a novel intravenous inotropic and lusitropic agent: a randomized controlled trial in patients hospitalized with heart failure. *J Am Coll Cardiol* **51**:2276–2285.
 Gwathmey JK, Copelas L, MacKinnon R, Schoen FJ, Feldman MD, Grossman W, and Morgan JP (1987) Abnormal intracellular calcium handling in myocardium from patients with end-stage heart failure. *Circ Res* **61**:70–76.
 Haghighi K, Schmidt AG, Hoit BD, Brittsan AG, Yatani A, Lester JW, Zhai J, Kimura Y, Dorn GW, MacLennan DH, et al. (2001) Superinhibition of sarcoplasmic reticulum function by phospholamban induces cardiac contractile failure. *J Biol Chem* **276**:24145–24152. DOI: 10.1074/jbc.M102403200.
 Kaneko M, Yamamoto H, Sakai H, Kamada Y, Tanaka T, Fujiwara S, Yamamoto S, Takahagi H, Igawa H, Kasai S, et al. (2017) A pyridone derivative activates SERCA2a by attenuating the inhibitory effect of phospholamban. *Eur J Pharmacol* **814**:1–8.
 Kho C, Lee A, Jeong D, Oh JG, Chaanine AH, Kizana E, Park WJ, and Hajjar RJ (2011) SUMO1-dependent modulation of SERCA2a in heart failure. *Nature* **477**:601–605.
 Kranias EG and Hajjar RJ (2012) Modulation of cardiac contractility by the phospholamban/SERCA2a regulatome. *Circ Res* **110**:1646–1660.
 Lang RM, Bierig M, Devereux RB, Flachskampf FA, Foster E, Pellikka PA, Picard MH, Roman MJ, Seward J, Shanewise J, et al.; American Society of Echocardiography's Nomenclature and Standards Committee; Task Force on Chamber Quantification; American College of Cardiology Echocardiography Committee; American Heart Association; European Association of Echocardiography, European Society of Cardiology (2006) Recommendations for chamber quantification. *Eur J Echocardiogr* **7**:79–108.
 Micheletti R, Mattera GG, Rocchetti M, Schiavone A, Loi MF, Zaza A, Gagnoli RJP, De Munari S, Melloni P, Carminati P, et al. (2002) Pharmacological profile of the novel inotropic agent (E,Z)-3-((2-aminoethoxy)imino)androstane-6,17-dione hydrochloride (PST2744). *J Pharmacol Exp Ther* **303**:592–600.
 Micheletti R, Palazzo F, Barassi P, Giacalone G, Ferrandi M, Schiavone A, Moro B, Parodi O, Ferrari P, and Bianchi G (2007) Istaroxime, a stimulator of sarcoplasmic reticulum calcium adenosine triphosphatase isoform 2a activity, as a novel therapeutic approach to heart failure. *Am J Cardiol* **99** (2A):24A–32A.
 Mihm MJ, Seifert JL, Coyle CM, and Bauer JA (2001) Diabetes related cardiomyopathy time dependent echocardiographic evaluation in an experimental rat model. *Life Sci* **69**:527–542.
 Mossahebi S, Zhu S, and Kovács SJ (2015) Fractionating E-wave deceleration time into its stiffness and relaxation components distinguishes pseudonormal from normal filling. *Circ Cardiovasc Imaging* **8**:e002177.
 Nakayama H, Chen X, Baines CP, Klevisky R, Zhang X, Zhang H, Jaleel N, Chua BHL, Hewett TE, Robbins J, et al. (2007) Ca^{2+} and mitochondrial-dependent cardiomyocyte necrosis as a primary mediator of heart failure. *J Clin Invest* **117**:2431–2444.
 Odening KE, Gomez A-M, Dobrev D, Fabritz L, Heinzel FR, Mangoni ME, Molina CE, Sacconi L, Smith G, Stengl M, et al. (2021) ESC working group on cardiac cellular electrophysiology position paper: relevance, opportunities, and limitations of experimental models for cardiac electrophysiology research. *Europace* **23**:1795–1814.
 Rocchetti M, Besana A, Mostacciolo G, Ferrari P, Micheletti R, and Zaza A (2003) Diverse toxicity associated with cardiac Na^+/K^+ pump inhibition: evaluation of electrophysiological mechanisms. *J Pharmacol Exp Ther* **305**:765–771.
 Rocchetti M, Besana A, Mostacciolo G, Micheletti R, Ferrari P, Sarkozi S, Szegedi C, Jona I, and Zaza A (2005) Modulation of sarcoplasmic reticulum function by Na^+/K^+ pump inhibitors with different toxicity: digoxin and PST2744 [(E,Z)-3-((2-aminoethoxy)imino)androstane-6,17-dione hydrochloride]. *J Pharmacol Exp Ther* **313**:207–215.
 Sabbah HN, Imai M, Cowart D, Amato A, Carminati P, and Gheorghiade M (2007) Hemodynamic properties of a new-generation positive ino-inotropic agent for the acute treatment of advanced heart failure. *Am J Cardiol* **99** (2A):41A–46A.
 Schaaf TM, Kleinboehl E, Yuen SL, Roelike LN, Svensson B, Thompson AR, Cornea RL, and Thomas DD (2020) Live-Cell Cardiac-Specific High-Throughput Screening Platform for Drug-Like Molecules that Enhance Ca^{2+} Transport. *Cells* **9**:1170.

- Shah SJ, Blair JEA, Filippatos GS, Macarie C, Ruzyllo W, Korewicki J, Bubenek-Turconi SI, Ceracchi M, Bianchetti M, Carminati P, et al.; HORIZON-HF Investigators (2009) Effects of istaroxime on diastolic stiffness in acute heart failure syndromes: results from the Hemodynamic, Echocardiographic, and Neurohormonal Effects of Istaroxime, a Novel Intravenous Inotropic and Lusitropic Agent: a Randomized Controlled Trial in Patients Hospitalized with Heart Failure (HORIZON-HF) trial. *Am Heart J* **157**:1035–1041.
- Shannon TR, Chu G, Kranias EG, and Bers DM (2001) Phospholamban decreases the energetic efficiency of the sarcoplasmic reticulum Ca pump. *J Biol Chem* **276**:7195–7201.
- Shiels HA and White E (2008) The Frank-Starling mechanism in vertebrate cardiac myocytes. *J Exp Biol* **211**:2005–2013. DOI: 10.1242/jeb.003145.
- Suko J, Vogel JHK, and Chidsey CA (1970) Intracellular calcium and myocardial contractility. 3. Reduced calcium uptake and ATPase of the sarcoplasmic reticular fraction prepared from chronically failing calf hearts. *Circ Res* **27**:235–247.
- Sulakhe PV and Dhalia NS (1971) Excitation-contraction coupling in heart. VII. Calcium accumulation in subcellular particles in congestive heart failure. *J Clin Invest* **50**:1019–1027.
- Tobushi T, Nakano M, Hosokawa K, Koga H, and Yamada A (2017) Improved diastolic function is associated with higher cardiac output in patients with heart failure irrespective of left ventricular ejection fraction. *J Am Heart Assoc* **6**:e003389.
- Torre E, Arici M, Lodrini AM, Ferrandi M, Barassi P, Hsu S-C, Chang G-J, Boz E, Sala E, Vagni S, et al. (2022) SERCA2a stimulation by istaroxime improves intracellular Ca²⁺ handling and diastolic dysfunction in a model of diabetic cardiomyopathy. *Cardiovasc Res* **118**:1020–1032. DOI: 10.1093/cvr/cvab123.
- Tournoux F, Petersen B, Thibault H, Zou L, Rahe MJ, Kurtz B, Halpern EF, Chaput M, Chao W, Picard MH, et al. (2011) Validation of noninvasive measurements of cardiac output in mice using echocardiography. *J Am Soc Echocardiogr* **24**:465–470.
- Valero-Muñoz M, Backman W, and Sam F (2017) Murine Models of Heart Failure with Preserved Ejection Fraction: a “Fishing Expedition”. *JACC Basic Transl Sci* **2**:770–789.
- Zaza A and Rocchetti M (2015) Calcium store stability as an antiarrhythmic endpoint. *Curr Pharm Des* **21**:1053–1061.

Address correspondence to: Dr. Marcella Rocchetti, Dipartimento di Biotecnologie e Bioscienze, Università degli Studi di Milano-Bicocca, P.za della Scienza 2, 2016 Milano, Italy. E-mail: marcella.rocchetti@unimib.it; or Dr. Antonio Zaza, FESC, Dipartimento di Biotecnologie e Bioscienze, Università degli Studi di Milano-Bicocca, P.za della Scienza 2, 2016 Milano, Italy. E-mail: antonio.zaza@unimib.it

SUPPLEMENTAL DATA

Journal of Pharmacology and Experimental Therapeutics

Manuscript number: JPET-AR-2022-001335

“Istaroxime metabolite PST3093 selectively stimulates SERCA2a and reverses disease-induced changes in cardiac function” by Arici M & Ferrandi M et al.

Index

Supplementary Methods	p. 2
Supplementary Figures and Tables:	pp. 5-13
Figure S1: Protocol to evaluate intracellular Ca^{2+} dynamics in patch-clamped cells under Na^+ free condition;	p. 5
Figure S2: Analytical characterization of PST3093;	pp. 6-7
Figure S3: Effects of 1 μM PST3093 on electrical activity in guinea-pig myocytes;	p. 8
Table S1: Effect of PST3093 and istaroxime on SERCA2a kinetic parameters in cardiac preparations from healthy guinea-pigs;	p. 9
Table S2: Effect of PST3093 (10 μM) on the panel of molecular targets;	pp. 10-11
Table S3: Characterization of the STZ diabetic rat model;	p. 12
Table S4: Echocardiographic parameters in healthy and STZ diabetic rats	p. 13

Supplementary Methods

Animal models

Male Sprague Dawley (SD) rats (150-175 gr) were used to generate STZ-induced diabetic cardiomyopathy model to test compounds *in vivo* and *in vitro*; female Dunkin-Hartley guinea pigs (175-200 g) were used for cardiac and skeletal muscle preparations (male 450-500 g) and myocytes isolation and finally, male Albino Swiss CD1 mice (30 g) were used for acute *in vivo* toxicity.

Pharmacodynamics 1: effect on SERCA2a and Na⁺/K⁺ ATPase activities in cell-free preparations (enzymatic assays)

Renal Na⁺/K⁺ ATPase purification and activity. Purification of renal Na⁺/K⁺ ATPase was performed according to the method of Jørgensen (Jørgensen, 1988). Frozen kidneys from 1-3 years-old male beagle dogs were obtained from the General Pharmacology Department of Sigma-tau, Pomezia, Italy. Kidneys were sliced and the outer medulla was dissected, pooled and suspended in a sucrose-histidine solution, containing 250 mM sucrose, 30 mM histidine and 5 mM EDTA, pH 7.2 and homogenized. The homogenate was centrifuged at 6,000 g for 15 min, the supernatant was decanted and centrifuged at 48,000 g for 30 min. The pellet was suspended in the sucrose-histidine buffer and incubated for 20 min with a sodium-dodecyl-sulphate (SDS) solution, dissolved in a gradient buffer, containing 25 mM imidazole and 1 mM EDTA, pH 7.5. The sample was layered on the top of a sucrose discontinuous gradient (10, 15 and 29.4%) and centrifuged at 60,000 g for 115 min. The final pellet was suspended in the gradient buffer. Na⁺/K⁺ ATPase activity was assayed by measuring ³²P-ATP hydrolysis, as previously described (Ferrandi *et al.*, 1996). Increasing concentrations of the standard ouabain, or tested compound, were incubated with 0.3 µg of purified dog kidney enzyme for 10 min at 37°C in 120 µl final volume of a medium, containing 140 mM NaCl, 3 mM MgCl₂, 50 mM Hepes-Tris, 3 mM ATP, pH 7.5. Then, 10 µl of incubation solution containing 10 mM KCl and 20 nCi of ³²P-ATP (3-10 Ci/mmol, Perkin Elmer) were added, the reaction continued for 15 min at 37°C and was stopped by acidification with 20% ice-cold perchloric acid. ³²P was separated by centrifugation with activated Charcoal (Norit A, Serva) and the radioactivity was measured. Effects of increasing concentrations of the test compound were compared to ouabain, as positive standard, and to vehicle (control) at 37°C. The inhibitory activity was expressed as percent of activity in control.

SERCA ATPase activity assay. LV were dissected from rat and guinea pig of healthy and failing preparations and frozen until use. Tissues were homogenized, subjected to centrifugation to obtain SR-enriched microsomes and sarcomeric proteins were extracted, as previously described (Micheletti *et al.*, 2007). In the case of rat hearts, cardiac homogenates were used in order to have sufficient material to replicate the experiments within a single animal. LV tissues from healthy and STZ rats were homogenized in a medium containing 300 mM sucrose, 50 mM K-phosphate, 10 mM NaF, 0.3 mM PMSF, 0.5 mM DTT (pH 7) and centrifuged at 35,000 g for 30 min. The final pellet was resuspended in the same buffer. In the case of guinea-pig hearts, LV tissues were homogenized in 4 volumes of 10 mM NaHCO₃, 1 mM PMSF, 10 µg/ml aprotinin and leupeptin (pH 7) and centrifuged at 12,000g for 15 minutes. Supernatants were filtered and centrifuged at 100,000 g for 30 min. Contractile proteins were extracted by suspending the pellets with 0.6 M KCl, 30 mM histidine, pH 7 and further centrifugation at 100,000 g for 30 min. Final pellets were reconstituted with 0.3 M sucrose, 30 mM histidine, pH 7, to obtain SR-enriched microsomes. SERCA2a ATPase activity was measured as the rate of ³²P-ATP release at multiple Ca²⁺ concentrations in the absence and presence of test compounds, as previously described (Micheletti *et al.*, 2007). Increasing concentrations of each compound were pre-incubated with 2 µg of cardiac preparations for 5 min at 4° C in 80 µl of a solution containing 100

mM KCl, 5 mM MgCl₂, 1 μ M A23187, 20 mM Tris, pH 7.5. Then, 20 μ l of 5 mM Tris-ATP containing 50 nCi of ³²P-ATP (3-10 Ci/mmol, Perkin Elmer) were added. The ATP hydrolysis was continued for 15 min at 37°C and the reaction was stopped by acidification with 100 μ l of 20% ice-cold perchloric acid. ³²P was separated by centrifugation with activated charcoal (Norit A, Serva) and the radioactivity was measured.

Reconstitution of SERCA1 with PLN₁₋₃₂ synthetic fragment. Adult healthy guinea-pigs were used to prepare SERCA1-enriched SR microsomes from fast-twitch hind leg muscles. Microsomes were prepared as described for SERCA2a preparations. For reconstitution experiments, SERCA1 (PLN-free) was pre-incubated with synthetic PLN₁₋₃₂ fragment (canine sequence, Biomartik Corporation, Canada) in 20 mM imidazole, pH 7, at 1:300 SERCA1:PLN ratio for 30 min at room temperature. After pre-incubation, SERCA1 (PLN-free) alone, or reconstituted with PLN₁₋₃₂ fragment, was utilized for SERCA activity measurement by using ³²P-ATP hydrolysis method at different Ca²⁺ concentrations in the absence and presence of increasing concentrations of tested compounds, as described for SERCA2a ATPase activity.

Pharmacodynamics 2: in-vitro effects for ligands potentially accounting for off-target actions

Analysis of PST3093 interaction with a panel of 50 ligands was carried out by Eurofins (Taiwan) on crude membrane preparations according to Eurofins described procedures. The assay is partly based on radioligand displacement (e.g. for receptors) and partly on spectrophotometric detection of change in function (e.g. for enzymes). Results were compared to appropriate reference standards; a >50% change in affinity or activity was considered as a positive hit (interaction present).

Pharmacodynamics 3: effect on Na⁺/K⁺ ATPase current and intracellular Ca²⁺ dynamics

Rat and guinea-pig LV ventricular myocytes were isolated by using a retrograde coronary perfusion method previously published (Rocchetti *et al.*, 2003) with minor modifications. Rod-shaped, Ca²⁺-tolerant myocytes were used within 12 h from dissociation. LV myocytes were clamped in the whole-cell configuration (Axopatch 200A, Axon Instruments Inc., Union City, CA). During measurements, myocytes were superfused at 2 ml/min with Tyrode's solution containing 154 mM NaCl, 4 mM KCl, 2 mM CaCl₂, 1 mM MgCl₂, 5 mM HEPES/NaOH, and 5.5 mM D-glucose, adjusted to pH 7.35. A thermostated manifold, allowing for fast (electronically timed) solution switch, was used for cell superfusion. All measurements were performed at 35 °C. The pipette solution contained 110 mM K⁺ - aspartate, 23 mM KCl, 0.2 mM CaCl₂ (10⁻⁷ M calculated free-Ca²⁺ concentration), 3 mM MgCl₂, 5 mM HEPES-KOH, 0.5 mM EGTA-KOH, 0.4 mM GTP-Na⁺ salt, 5 mM ATP-Na⁺ salt, and 5 mM creatine phosphate Na⁺ salt, pH 7.3. Membrane capacitance and series resistance were measured in every cell but left uncompensated. Current signals were filtered at 2 KHz and digitized at 5 KHz (Axon Digidata 1200). Trace acquisition and analysis was controlled by dedicated software (Axon pClamp 8.0).

Na⁺/K⁺ ATPase current (I_{NaK}) measurements. I_{NaK} was recorded in isolated rat LV myocytes (Rocchetti *et al.*, 2003; Alemanni *et al.*, 2011) as the holding current recorded at -40 mV in the presence of Ni²⁺ (5 mM), nifedipine (5 μ M), Ba²⁺ (1 mM) and 4-aminopyridine (2 mM) to minimize contamination by changes in Na⁺/Ca²⁺ exchanger (NCX), Ca²⁺ and K⁺ currents, respectively. Tetraethylammonium-Cl (20 mM) and EGTA (5 mM) were added to the pipette solution and intracellular K⁺ was replaced by Cs⁺. To optimize the recording conditions, I_{NaK} was enhanced by increasing intracellular Na⁺ (10 mM) and extracellular K⁺ (5.4 mM). All drugs were dissolved in dimethyl sulfoxide (DMSO). Control and test solutions contained maximum 1:100 DMSO.

Intracellular Ca^{2+} dynamics. LV myocytes were incubated in Tyrode's solution for 30 min with the membrane-permeant form of the dye, Fluo4-AM (10 μM), and then washed for 15 min to allow dye de-esterification. Fluo4 emission was collected through a 535 nm band pass filter, converted to voltage, low-pass filtered (100 Hz) and digitized at 2 kHz after further low-pass digital filtering (FFT, 50 Hz). After subtraction of background luminescence, a reference fluorescence (F_0) value was used for signal normalization (F/F_0). Cytosolic Ca^{2+} activity was dynamically measured in field stimulated (2 Hz) and patch-clamped rat LV myocytes. In the first case, fluorescence in diastole was used as F_0 for signal normalization (F/F_0).

In patch-clamped myocytes membrane current, whose time-dependent component mainly reflected the sarcolemmal Ca^{2+} current (I_{CaL}), was simultaneously recorded. Drug effects on SR Ca^{2+} uptake rate were evaluated with a "SR loading protocol" specifically devised to rule out the contribution of NCX and to assess the SR Ca^{2+} uptake rate at multiple levels of SR Ca^{2+} loading (Rocchetti *et al.*, 2005) (protocol in Figure S1). The protocol consisted in emptying the SR by a brief caffeine (10 mM) pulse and then progressively refilling it by 7-10 voltage steps (-35 to 0 mV) activating Ca^{2+} influx through I_{CaL} . NCX was blocked by omission of Na^+ from intracellular and extracellular (replaced by equimolar Li^+ and 1 mM EGTA) solutions. The procedure is in agreement with published methods, with minor modifications (Rocchetti *et al.*, 2005; Alemanni *et al.*, 2011; Torre *et al.*, 2021). Multiple parameters, suitable to quantify SR Ca^{2+} uptake, can be extracted from Ca^{2+} and I_{CaL} response to the protocol: the time constant (τ) of cytosolic Ca^{2+} decay within each V-step largely reflects net Ca^{2+} flux across the SR membrane (the faster SR Ca^{2+} uptake, the smaller τ decay). Because of the steep dependency of CaT amplitude on SR Ca^{2+} content, the rate at which CaT amplitude increases across the subsequent pulses of the protocol reflects the rate at which the SR refills. To rule out the potential contribution of changes in I_{CaL} , in each loading step, CaT amplitude was normalized to Ca^{2+} influx (estimated from I_{CaL} integral up to CaT peak) to obtain excitation-release (ER) gain. As expected from its strong dependency on SR Ca^{2+} content, this parameter progressively increases during the loading protocol. Diastolic Ca^{2+} of the first step was used as F_0 for signal normalization (F/F_0). Specificity of the "loading protocol" parameters in detecting SERCA2a activation is supported by the observation that they did not detect any effect of digoxin, an inotropic agent blocking the Na^+/K^+ pump and devoid of SERCA2a stimulating effect (Rocchetti *et al.*, 2005; Alemanni *et al.*, 2011).

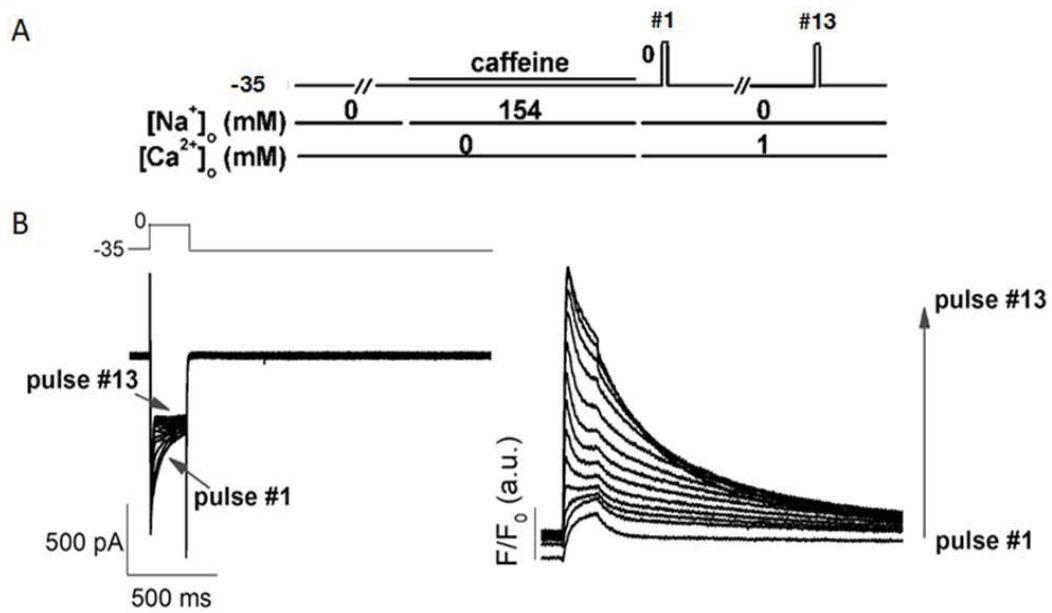
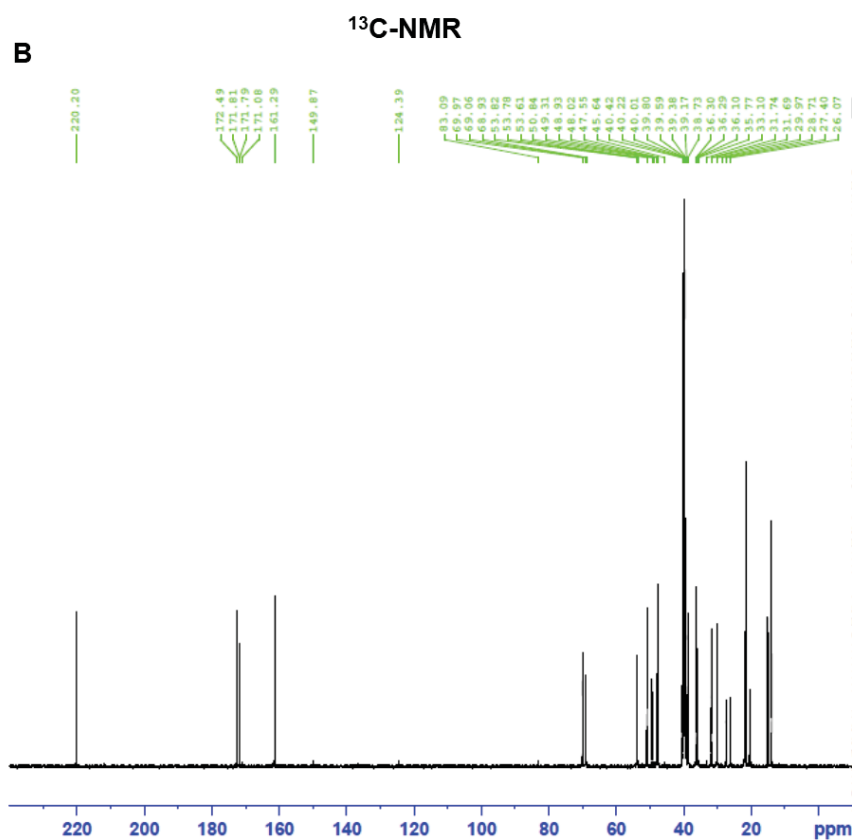
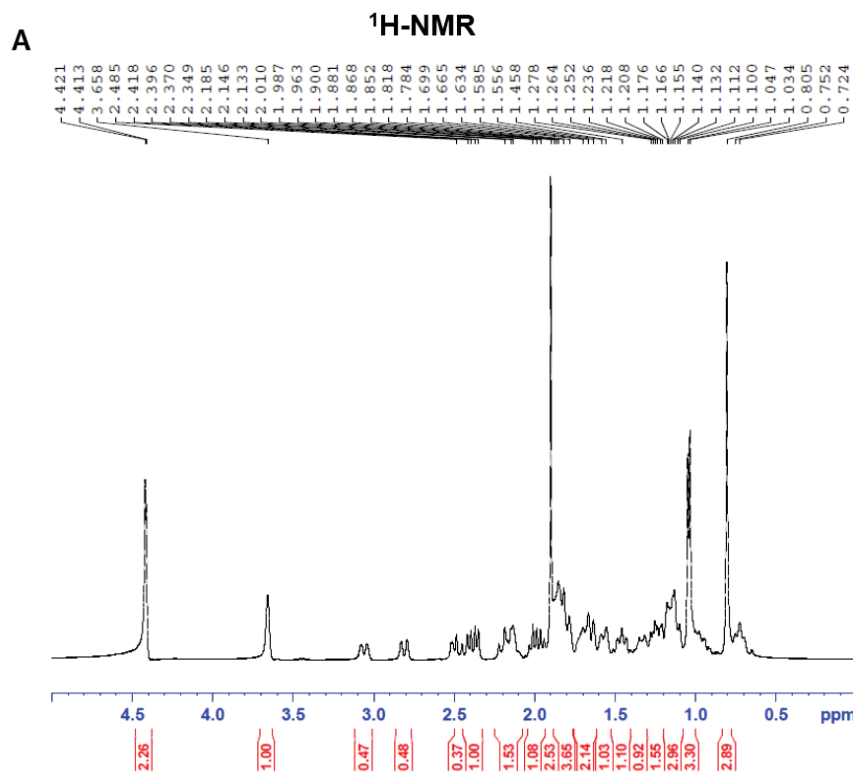


Figure S1. Protocol to evaluate intracellular Ca^{2+} dynamics in patch-clamped cells under Na^+ free condition. **A)** Protocol outline. **B)** Transmembrane current (left) and Ca^{2+} transients (right) recordings during SR reloading after caffeine-induced SR depletion in patch-clamped cells. See Methods for details.



C

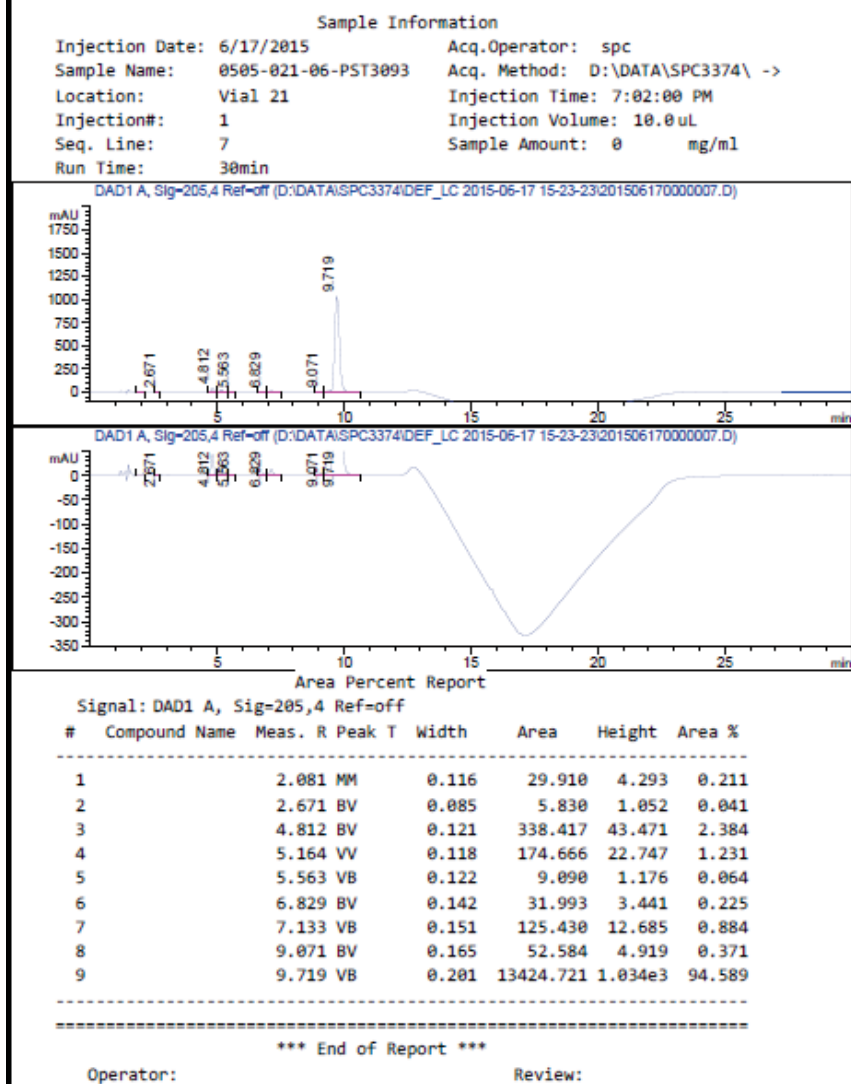


Figure S2. Analytical characterization of PST3093. A) ^1H -NMR in DMSO (400 MHz, Bruker), B) ^{13}C -NMR in DMSO (100 MHz, Bruker), C) HPLC profile (about 95% purity).

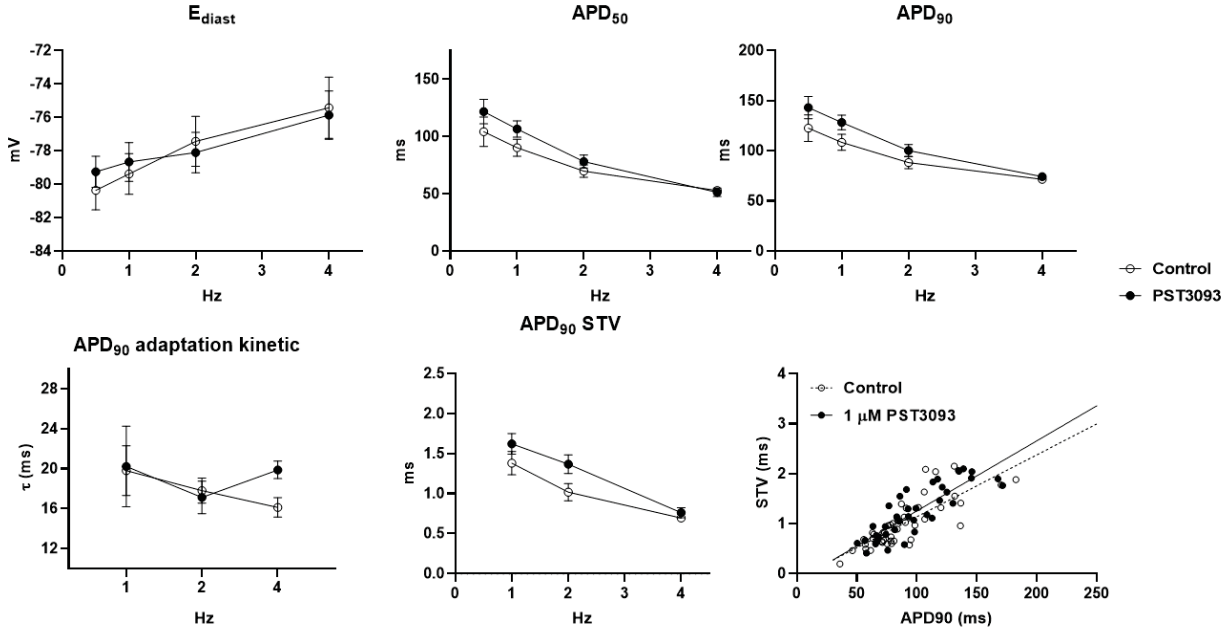


Figure S3. Effects of 1 μ M PST3093 on electrical activity in guinea-pig myocytes. Rate dependency of AP parameters (E_{diast} , APD_{50} , APD_{90}), APD_{90} adaptation kinetics and APD_{90} short term variability (STV) with or w/o 1 μ M PST3093; N=3 (n=16 w/o PST3093, n=18 with PST3093). Bottom right: linear correlation between STV of APD_{90} and APD_{90} values with or w/o PST3093; data from 1, 2, 4 Hz were pooled (w/o PST3093 slope = 0.012, with PST3093 slope = 0.014, NS).

Table S1. Effect of PST3093 and istaroxime on SERCA2a kinetic parameters in cardiac preparations from healthy guinea-pigs. Data are mean \pm SEM; N indicates the number of experiments. *p<0.05 vs control (RM one-way ANOVA with post-hoc Tukey's multiple comparisons test or paired *t*-test).

Guinea-pigs						
[nM]	N	control	PST3093	N	control	istaroxime
V _{max} (μmol/min/mg)						
1	9	2,28±0,17	2,16±0,18	9	2,51±0,08	2,50±0,04
10			2,15±0,15			2,47±0,06
100	11	2,38±0,16	2,34±0,16			2,49±0,07
K _d Ca (nM)						
1	9	567±12	504±23*	9	584±22	524±19
10			501±17*			485±16*
100	11	557±12	445±30*			478±19*

Table S2. Effect of PST3093 (10 μ M) on the panel of molecular targets (Eurofins, Taiwan).

	Cat #	Assay name	Batch	Species	PST3093 effect (%)
1	107480	ATPase, Ca ²⁺ , skeletal muscle	438642	pig	-18
2	118040	CYP450, 19	438644	human	12
3	124010	HMG-CoA Reductase	438610	human	-2
4	140010	Monoamine Oxidase MAO-A	438645	human	2
5	140120	Monoamine Oxidase MAO-B	438647	human	-3
6	143000	Nitric Oxide Synthase, Endothelial (eNOS)	438568	bovine	2
7	107300	Peptidase, Angiotensin Converting Enzyme	438641	rabbit	3
8	164610	Peptidase, Renin	438648	human	6
9	152000	Phosphodiesterase PDE3	438611	human	-3
10	171601	Protein Tyrosine Kinase, ABL1	438612	human	3
11	176810	Protein Tyrosine Kinase, Src	438613	human	-1
12	200510	Adenosine A1	438614	human	-2
13	200610	Adenosine A2A	438614	human	-6
14	203100	Adrenergic α 1A	438615	rat	2
15	203200	Adrenergic α 1B	438615	rat	0
16	203630	Adrenergic α 2A	438616	human	-5
17	204010	Adrenergic β 1	438652	human	-4
18	204110	Adrenergic β 2	438571	human	7
19	204600	Aldosterone	438617	rat	5
20	206000	Androgen (Testosterone)	438618	human	3
21	210030	Angiotensin AT1	438653	human	-1
22	210120	Angiotensin AT2	438653	human	7
23	214600	Calcium Channel L-type, Dihydropyridine	438620	rat	-8
24	219500	Dopamine D1	438660	human	3

25	219700	Dopamine D2s	439024	human	26
26	219800	Dopamine D3	438660	human	1
27	226010	Estrogen ER α	438622	human	-6
28	226050	Estrogen ER β	438622	human	7
29	226600	GABA _A , Flunitrazepam, Central	438624	rat	4
30	226500	GABA _A , Muscimol, Central	438623	rat	9
31	232030	Glucocorticoid	438626	human	8
32	233000	Glutamate, NMDA, Phencyclidine	438627	rat	-8
33	239610	Histamine H1	438628	human	-3
34	241000	Imidazoline I2, Central	438629	rat	5
35	243000	Insulin	438654	rat	6
36	252710	Muscarinic M2	438621	human	-7
37	252810	Muscarinic M3	438661	human	4
38	253010	Muscarinic M5	438661	human	5
39	258730	Nicotinic Acetylcholine $\alpha 3\beta 4$	438656	human	1
40	260410	Opiate μ (OP3, MOP)	438616	human	-5
41	264500	Phorbol Ester	438624	mouse	-7
42	265600	Potassium Channel (K _{ATP})	438632	hamster	-8
43	265900	Potassium Channel hERG	438633	human	10
44	299005	Progesterone PR-B	438638	human	-15
45	270300	Ryanodine RyR3	438634	rat	2
46	271010	Serotonin (5-Hydroxytryptamine) 5-HT1, non-selective	438668	rat	0
47	299007	Sigma $\sigma 2$	438662	human	12
48	278110	Sigma $\sigma 1$	438636	human	7
49	279510	Sodium Channel, Site 2	438637	rat	2
50	204410	Transporter, Norepinephrine (NET)	438597	human	4

Table S3. Characterization of the STZ diabetic rat model. Parameters were measured after 1 or 8 weeks (wk) from STZ injection. Data are mean \pm SEM. N represents the number of rats for each group. *p<0.05 vs healthy rats (unpaired *t*-test).

	Healthy		STZ	
Parameters	1 wk after vehicle	8 wk after vehicle	1 wk after STZ	8 wk after STZ
BW (g)	201 \pm 4.7	449 \pm 11.8	193 \pm 4.2	305 \pm 12.9*
Glycaemia (mg/dL)	130 \pm 6.6	nd	398 \pm 16*	nd
LV mass (mm ³)	nd	985 \pm 34	nd	781 \pm 40*
LV mass index (mm ³ /g)	nd	2,23 \pm 0,1	nd	2,66 \pm 0,2
N	18	18	20	20

Table S4. Echocardiographic parameters in healthy and STZ diabetic rats. Data are mean \pm SEM. N represents the number of rats for each group. * $p < 0.05$ vs healthy rats (unpaired t -test).

Echo parameters		Healthy	STZ
Morphometric parameters	IVSTd (mm)	2,22 \pm 0,07	1,73 \pm 0,1 *
	PWTd (mm)	1,87 \pm 0,09	1,54 \pm 0,05 *
	LVEDD (mm)	6,6 \pm 0,14	6,95 \pm 0,13
	IVSTs (mm)	2,46 \pm 0,07	2,26 \pm 0,1
	PWTs (mm)	2,96 \pm 0,09	2,47 \pm 0,11 *
	LVESD (mm)	3,09 \pm 0,09	3,54 \pm 0,1 *
Systolic parameters	FS (%)	53,08 \pm 1,17	48,73 \pm 1,37 *
	s' (mm/s)	29,59 \pm 1,15	24,8 \pm 0,75 *
	EF (%)	88 \pm 0,8	85 \pm 1,08 *
Diastolic parameters	E (mm/s)	0,93 \pm 0,01	0,84 \pm 0,02 *
	A (mm/s)	0,65 \pm 0,04	0,63 \pm 0,03
	E/A	1,50 \pm 0,08	1,38 \pm 0,07
	DT (ms)	54,61 \pm 2,1	56,8 \pm 2,16
	DT/E	59,23 \pm 2,4	68,37 \pm 3,0 *
	E/DT	17,41 \pm 0,77	15,18 \pm 0,67 *
	e' (mm/s)	23,46 \pm 0,77	21,34 \pm 0,58 *
	a' (mm/s)	24,54 \pm 1,38	24,3 \pm 1,13
	e'/a'	1,01 \pm 0,06	0,91 \pm 0,04
	E/e'	40,1 \pm 1,33	39,64 \pm 1,0
Overall cardiac function	HR (bpm)	306 \pm 10	248 \pm 7,4 *
	LV EDV (mL)	0.67 \pm 0.04	0.77 \pm 0.04
	LV ESV (mL)	0.08 \pm 0.01	0.12 \pm 0.01 *
	SV (ml)	0,59 \pm 0,03	0,65 \pm 0,04
	CO (ml/min)	178,9 \pm 10,2	161,1 \pm 10,9
	N	18	20

References

- Alemanni M, Rocchetti M, Re D, and Zaza A (2011) Role and mechanism of subcellular Ca^{2+} distribution in the action of two inotropic agents with different toxicity. *J Mol Cell Cardiol* **50**:910–918.
- Ferrandi M, Tripodi G, Salardi S, Florio M, Modica R, Barassi P, Parenti P, Shainskaya A, Karlisch S, Bianchi G, and Ferrari P (1996) Renal Na,K -ATPase in genetic hypertension. *Hypertension* **28**:1018–1025.
- Jørgensen PL (1988) Purification of $\text{Na}^{+},\text{K}^{+}$ -ATPase: Enzyme Sources, Preparative Problems, And Preparation from Mammalian Kidney. *Methods Enzymol* **156**:29–43.
- Micheletti R, Palazzo F, Barassi P, Giacalone G, Ferrandi M, Schiavone A, Moro B, Parodi O, Ferrari P, and Bianchi G (2007) Istaroxime, a Stimulator of Sarcoplasmic Reticulum Calcium Adenosine Triphosphatase Isoform 2a Activity, as a Novel Therapeutic Approach to Heart Failure. *Am J Cardiol* **99**:24A-32A.
- Rocchetti M, Besana A, Mostacciuolo G, Ferrari P, Micheletti R, and Zaza A (2003) Diverse toxicity associated with cardiac $\text{Na}^{+}/\text{K}^{+}$ pump inhibition: Evaluation of electrophysiological mechanisms. *J Pharmacol Exp Ther* **305**:765–771.
- Rocchetti M, Besana A, Mostacciuolo G, Micheletti R, Ferrari P, Sarkozi S, Szegedi C, Jona I, and Zaza A (2005) Modulation of sarcoplasmic reticulum function by $\text{Na}^{+}/\text{K}^{+}$ pump inhibitors with different toxicity: Digoxin and PST2744 [(E,Z)-3-((2-aminoethoxy)imino)androstane-6,17-dione hydrochloride]. *J Pharmacol Exp Ther* **313**:207–215.
- Torre E, Arici M, Lodrini AM, Ferrandi M, Barassi P, Hsu S-C, Chang G-J, Boz E, Sala E, Vagni S, Altomare C, Mostacciuolo G, Bussadori C, Ferrari P, Bianchi G, and Rocchetti M (2021) SERCA2a stimulation by istaroxime improves intracellular Ca^{2+} handling and diastolic dysfunction in a model of diabetic cardiomyopathy. *Cardiovasc Res*, doi: 10.1093/cvr/cvab123, Oxford University Press (OUP).